

# Northumbria Research Link

Citation: Jamil, Muhammad Ahmad, Goraya, Talha S., Shahzad, Muhammad Wakil and Zubair, Syed M. (2020) Exergoeconomic optimization of a shell-and-tube heat exchanger. *Energy Conversion and Management*, 226. p. 113462. ISSN 0196-8904

Published by: Elsevier

URL: <https://doi.org/10.1016/j.enconman.2020.113462>  
<<https://doi.org/10.1016/j.enconman.2020.113462>>

This version was downloaded from Northumbria Research Link:  
<http://nrl.northumbria.ac.uk/id/eprint/45157/>

Northumbria University has developed Northumbria Research Link (NRL) to enable users to access the University's research output. Copyright © and moral rights for items on NRL are retained by the individual author(s) and/or other copyright owners. Single copies of full items can be reproduced, displayed or performed, and given to third parties in any format or medium for personal research or study, educational, or not-for-profit purposes without prior permission or charge, provided the authors, title and full bibliographic details are given, as well as a hyperlink and/or URL to the original metadata page. The content must not be changed in any way. Full items must not be sold commercially in any format or medium without formal permission of the copyright holder. The full policy is available online: <http://nrl.northumbria.ac.uk/policies.html>

This document may differ from the final, published version of the research and has been made available online in accordance with publisher policies. To read and/or cite from the published version of the research, please visit the publisher's website (a subscription may be required.)

# Exergoeconomic optimization of a shell-and-tube heat exchanger

Muhammad Ahmad Jamil<sup>a,b\*</sup>, Talha S. Goraya<sup>a</sup>, Muhammad Wakil Shahzad<sup>b</sup>, and Syed M. Zubair<sup>c\*</sup>

<sup>a</sup>Department of Mechanical Engineering, Khwaja Fareed University of Engineering and Information Technology, Rahim Yar Khan, Pakistan

<sup>b</sup>Mechanical & Construction Engineering Department, Northumbria University, Newcastle Upon Tyne, UK

<sup>c</sup>Mechanical Engineering Department, KFUPM Box # 1474 King Fahd University of Petroleum & Minerals, Dhahran 31261, Saudi Arabia

---

## **ABSTRACT**

The paper presents an economic optimization of STHX with two commonly adopted (i.e., Kern and Bell-Delaware) and one rarely explored (i.e., Wills-Johnston) methods. A detailed numerical code concerning thermal, hydraulic, exergy, and economic analysis of STHX is developed for all three methods. Normalized sensitivity analysis, parametric study, and Genetic Algorithm are used to ascertain the most influential parameters and optimize the total cost. It is observed that the calculations made using the Wills-Johnston method were reasonably close to the Bell-Delaware method. While the Kern method showed a significant deviation in the shell side calculations because of the several assumptions in this method. The parametric analysis showed that increasing the mass flow rate and the number of baffles increased the operating cost because of an exponential increase in the pressure drops. Finally, the optimization reduced the heat transfer area by ~26.4%, capital cost by ~20%, operational cost by ~50%, total cost by ~22%, and the stream cost by ~21%.

**Keywords:** shell and tube heat exchanger; exergoeconomic optimization; Kern; Bell-Delaware; Wills-Johnston; Genetic Algorithm

---

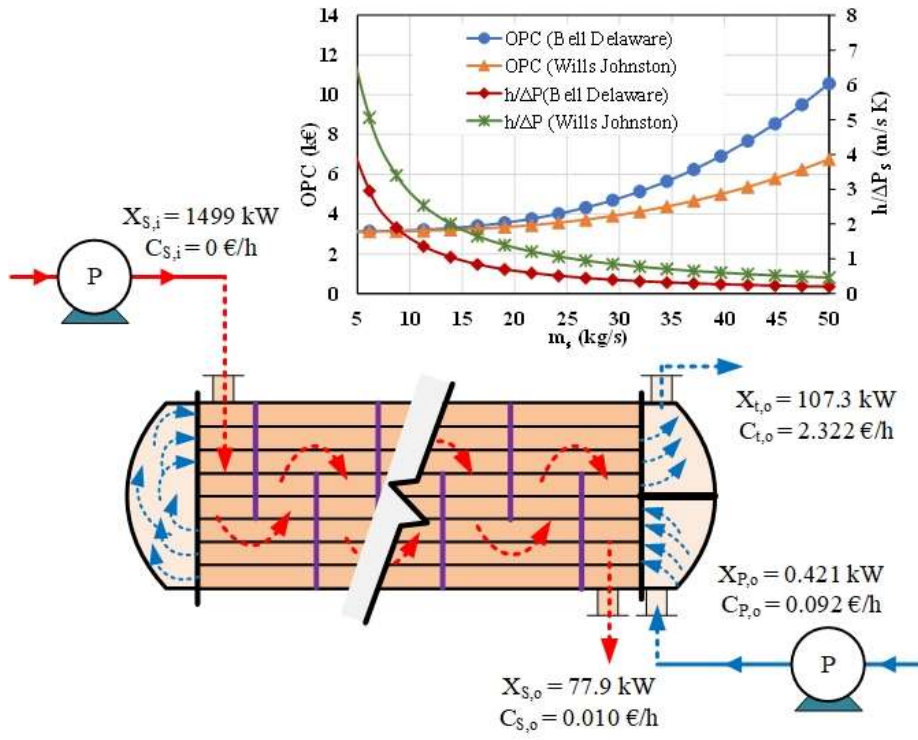
\* Corresponding author; e-mail: [ahmad.jamil@kfueit.edu.pk](mailto:ahmad.jamil@kfueit.edu.pk) (M.A. Jamil); [smzubair@kfpm.edu.sa](mailto:smzubair@kfpm.edu.sa) (S.M. Zubair);

25

### GRAPHICAL ABSTRACT

26

27



28

29

## 30 1. Introduction

31 The economic optimization of energy conversion systems is becoming inevitable with growing  
32 energy demands, cost-effective design, sustainable developments, and hikes in energy prices [1–  
33 3]. Heat exchangers not only play an important role as an integral part of almost every energy  
34 conversion system but also help to improve system efficiency by recovering heat from waste  
35 streams [4,5]. The most commonly used heat exchangers include shell-and-tube heat exchangers  
36 (STHX), gasketed plate heat exchangers, double pipe heat exchangers, and finned surface heat  
37 exchangers [6,7]. Among all, the STHXs are of particular importance and cover ~35-40% of the  
38 market because of larger heat transfer capabilities and high-pressure applications [8,9]. Therefore,  
39 the performance of these heat exchangers has been investigated extensively under varied operating  
40 conditions [10,11].

41 However, most of these studies are focused on improving thermal-hydraulic performance by  
42 varying geometric parameters such as baffle spacing, baffle orientation, the number of tubes, tube  
43 diameter. For instance, Jozaei et al. [12] reported that thermal-hydraulic performance decreases  
44 with increasing baffle spacing and suggested the range from 4 to 12 inches. Similarly, Abdelkader  
45 and Zubair [13] reported an increase in thermal-hydraulic performance with an increasing number  
46 of baffles. Furthermore, they reported that the heat transfer coefficient increased at a high rate  
47 when the square tube layout is used. Gao et al. [14] analyzed the effect of helical angle for  
48 discontinuous helical baffle STHX and reported that the helical angle with 40° provides the best  
49 comprehensive performance. Similarly, Abdelkader et al. [15] reported that the performance of a  
50 helical baffle HX decreased after the helix angle exceeded 42°.

51 Recently, researchers and industrialists have realized that STHXs optimization from a  
52 monetary viewpoint is also important together with conventional performance and design  
53 analysis [16,17]. It will have a great impact on overall system cost as they form a major portion of  
54 initial capital. For this purpose, various numerical approaches have been developed and used by  
55 the research community to minimize the total cost ( $C_{total}$ ) of STHXs, which include capital (CAPC)  
56 and operational cost (OPC). For example, Selbas et al. [18] used Genetic Algorithm to minimize  
57 the heat transfer area and cost. They reported that the GA can achieve significant improvement in  
58 the design compared to the conventional methods. Segundo et al. [19] proposed a falcon  
59 optimization algorithm and reported that the cost is reduced by 57.8% and effectiveness is  
60 increased by 10% for case 2. A critical review of some other recent studies conducted in this regard

61 is presented in Table 1. It is important to notice that, most of these studies have reported a  
62 considerable improvement in the performance of STHX by optimizing the objective functions such  
63 as effectiveness, heat transfer coefficients, pressure, and cost. However, there is another STHX  
64 analysis method “Flow Stream Analysis” or the Wills-Johnston method that has not been critically  
65 explored. Besides, most optimization techniques adopted in the studies presented in Table 1 are  
66 computationally expensive and require adequate knowledge and computational capacity.  
67 Therefore, analysis of STHX as an integral part of systems with multiple components e.g., power  
68 plants, desalination systems, cogeneration systems, etc. is not economical due to the combinatory  
69 effects of design variables and objective functions.

70 On the other hand, exergoeconomic analysis, a combined application of thermodynamics and  
71 economic analyses, is an important tool for thermal systems analysis [20]. It calculates the exergy  
72 and economic values of each fluid stream as it enters or leaves any component using capital and  
73 operational expenses, thus predicting the local product stream cost [21]. The product stream is  
74 defined based on a primary function of the equipment, e.g., for a pump, it is pressurized water; for  
75 a compressor, it is compressed vapor, and for an HX, it is hot/cold stream. Besides the calculation  
76 of local product cost, the analysis can also conduct design improvements and malfunctioning  
77 diagnosis [22]. This tool has already been used to improve systems like refrigeration [23],  
78 desalination [24–26], and heat recovery units [27]. It should be noted that a thorough exergo-  
79 economic design and optimization study of SHTX, is not covered in the above literature.

80 The current study is focused on developing and applying a systematic approach for exergy-  
81 and-cost flow-based analysis of STHXs. For this purpose, various design methods are critically  
82 examined for the thermal-hydraulic design of STHX. In addition, exergy analysis is conducted to  
83 calculate the flow exergy of all the streams as well as exergy destruction in the heat exchanger  
84 configuration. This is followed by an economic analysis that calculates various cost elements that  
85 applies to the current system. Also, the updated sensitivity of various influencing input parameters  
86 on the operational cost of HX is comprehensively investigated, in terms of normalized sensitivity  
87 coefficients. Finally, a cost optimum configuration is achieved by using the Genetic Algorithm.

88 To make the study useful for the readers, the manuscript is organized, systematically. In this  
89 regard, the first part is focused on the review of the economic optimization of STHX to identify  
90 the important parameters and their operating range. Section 2 covers the system description,  
91 governing equations, assumptions, and solution strategy. Thereafter in Section 3, the results and

92 discussion are presented. In Section 4 a general framework for the analysis of STHX as a preheater  
93 in a thermal desalination system is presented. Finally, the key findings are summarized in the last  
94 section.

95  
96

**Table 1.**  
Review of various studies on the economic optimization of STHXs using different algorithms.

Study	Method	Opt. Techniques	Objective	Constraints (min-max)	Outcome
Caputo et al. [28]	Kern	• Genetic Algorithm	• $C_{total}$	$D_{t,o}$ : 0.01-0.051 m, $D_s$ : 0.1-1.5 m $L_{bc}$ : 0.05-0.5 m	$\downarrow C_{total} (\leq 50\%)$
Guo et al. [29,30]	Bell-Delaware	• EGM • Field Synergy • Genetic Algorithm	• $S_{gen}$ • $\mathcal{E}$	$D_{t,o}$ : ASTM values, $B_c$ : 20-45% $N_t$ : 50-500, $L_{bc}/D_s$ : 201-100	$\downarrow C_{total}$ $\uparrow \mathcal{E}$
Ortega et al. [31]	Bell-Delaware	• Genetic Algorithm	• $C_{total}$	$D_{t,o}$ : ASTM values, $B_c$ :15-45%, $N_P$ : 1-8, $n_{pt}$ : 0-4, $\beta$ : 30° and 90° Fluid side allocation	$\downarrow C_{total} (\leq 33\%)$
Patel and Rao [32]	Kern	• Particle Swarm Optimization	• $C_{total}$	$D_{t,o}$ : 0.01-0.051 m, $D_s$ : 0.1-1.5 m $L_{bc}$ : 0.05-0.5 m, $\beta$ : 30° and 90°	$\downarrow C_{total} (4-5\%)$
Sahin et al. [33]	Kern	• Artificial Bee Colony Algorithm	• $C_{total}$	$N_t, D_{t,o}, L_t, L_{bc}, P_t$	$\downarrow C_{total} (\leq 55\%)$
Hadidi et al. [34]	Bell-Delaware	• Imperialist competitive algorithm	• $C_{total}$	$D_{t,o}$ : 0.01-0.051 m $D_s$ : 0.1-1.5 m, $L_{bc}$ : 0.05-0.5 m	$\downarrow C_{total} (\leq 53\%)$
Hadidi and Nazari [35]	Kern	• Biogeography-based algorithm	• $C_{total}$	$N_t, D_s, D_{t,o}, L_t, L_{bc}, P_t$	$\downarrow C_{total} (\leq 56\%)$
Asadi et al. [36]	Kern	• Cuckoo Search Algorithm.	• $C_{total}$	$D_{t,o}$ : 0.008-0.051m, $D_s$ : 0.2-0.9 m $L_{bc}$ : 0.05-0.5 m	$\downarrow CAPC (\leq 13\%)$ $\downarrow OPC (\leq 77\%)$
Sadeghzadeh et al. [37]	Kern Bell-Delaware	• Genetic Algorithms • Particle Swarm Optimization	• $C_{total}$	$D_{t,o}$ : 0.01-0.051 m, $D_s$ : 0.1-1.5 m $L_{bc}$ : 0.05-0.5 m	$\downarrow OPC (\leq 22\%)$
Khosravi et al. [38]	Bell-Delaware $\mathcal{E}-NTU$	• Genetic algorithm • Firefly algorithm • Cuckoo search algorithm	• $\mathcal{E}$ • $C_{total}$	$N_t$ : 100-600, $N_P$ : 1-3, $L_t$ : 3-8, $D_{t,i}$ : 0.0112-0.0172 m $L_{bc}$ : 0.2-1.4, $B_c$ : 0.19-0.32 (ratios) $P_t / D_{t,o}$ : 1.25-3, $\beta = 30^\circ - 90^\circ$	$\uparrow \mathcal{E} (\leq 83.8\%)$
Mohanty [39]	Kern	• Firefly Algorithm	• $C_{total}$	$N_t, D_s, D_{t,o}, L_t, L_{bc}$	$\downarrow C_{total} (\leq 29\%)$

Hajabdollahi et al. [40]	Bell-Delaware $\varepsilon-NTU$	<ul style="list-style-type: none"> <li>Genetic Algorithms</li> <li>Sensitivity Analysis</li> </ul>	<ul style="list-style-type: none"> <li><math>C_{total}</math></li> </ul>	$N_t$ : 100-600, $N_p$ : 1-3, $L_t$ : 3-8, $D_{t,i}$ : 0.0112-0.0172 m, $L_{bc}$ : 0.2-1.4, $B_c$ : 0.19-0.32 (ratios) $P_t / D_{t,o}$ : 1.25-3, $\beta = 30^\circ - 90^\circ$ Fluid side allocation	$\downarrow C_{total} (\leq 35\%)$
Dhavle et al. [41]	Kern	<ul style="list-style-type: none"> <li>Cohort Intelligence Algorithm</li> </ul>	<ul style="list-style-type: none"> <li><math>C_{total}</math></li> </ul>	$D_{t,o}$ : 0.01-0.051 m, $N_p$ : 1-8, $D_s$ : 0.1-1.5 m, $L_{bc}$ : 0.05-0.5 m	$\downarrow C_{total} (\leq 52\%)$
Wen et al. [42]	Helical Baffle Correlations	<ul style="list-style-type: none"> <li>Genetic Algorithm (Kriging Metamodel)</li> </ul>	<ul style="list-style-type: none"> <li><math>\dot{Q}</math></li> <li><math>C_{total}</math></li> </ul>	Helical angles Baffle overlap ratio Inlet volume flow rate	$\downarrow C_{total} (\leq 32\%)$
Rao and Siraj [43]	Towler and Sinnott	<ul style="list-style-type: none"> <li>Elitist-Jaya Algorithm</li> </ul>	<ul style="list-style-type: none"> <li><math>C_{total}</math></li> </ul>	$N_t, D_s, D_{t,o}, L_t, L_{bc}$	$\downarrow C_{total} (\leq 33\%)$
Segundo et al. [44]	Kern	<ul style="list-style-type: none"> <li>Tsallis Differential Evolution</li> </ul>	<ul style="list-style-type: none"> <li><math>C_{total}</math></li> </ul>	$D_s, D_{t,o}, L_{bc}$	$\downarrow C_{total} (\leq 54\%)$
Tharakeshwar et al. [45]	Bell-Delaware	<ul style="list-style-type: none"> <li>Genetic Algorithm</li> <li>Bat Algorithm</li> </ul>	<ul style="list-style-type: none"> <li><math>\mathcal{E}</math></li> <li><math>C_{total}</math></li> </ul>	$B_c, L_{bc}, P_t, L_t, \beta$	$\downarrow C_{total} (\leq 14\%)$
Mirzaei et al. [46]	$\varepsilon-NTU$	<ul style="list-style-type: none"> <li>Constructal Theory</li> <li>Genetic Algorithm</li> </ul>	<ul style="list-style-type: none"> <li><math>\mathcal{E}</math></li> <li><math>C_{total}</math></li> </ul>	$N_t, D_t, L_t$	$\uparrow \mathcal{E} (28\%)$ $\downarrow C_{total} (\leq 32\%)$
Iyer et al. [47]	Kern	<ul style="list-style-type: none"> <li>Adaptive Range Genetic Algorithm</li> </ul>	<ul style="list-style-type: none"> <li><math>C_{total}</math></li> </ul>	$D_{t,o}$ : 0.01-0.051 m, $D_s$ : 0.1-1.5 m $L_{bc}$ : 0.05-0.5 m, $N_p$ : 1-8	$\downarrow C_{total} (\leq 52\%)$
Sai and Rao [48]	Kern	<ul style="list-style-type: none"> <li>Bacteria Foraging Algorithm</li> </ul>	<ul style="list-style-type: none"> <li><math>\mathcal{E}</math></li> <li><math>C_{total}</math></li> </ul>	$D_{t,o}, D_s, L_{bc}, N_p$	$\downarrow C_{total} (\leq 2\%)$
Current study	Kern Bell-Delaware Wills Johnston	<ul style="list-style-type: none"> <li>Exergoeconomics</li> <li>Normalized Sensitivity Analysis</li> <li>Genetic Algorithm</li> </ul>	<ul style="list-style-type: none"> <li><math>h/\Delta P</math></li> <li>NSC</li> <li><math>X_D</math></li> <li><math>C_{total}</math></li> </ul>	Design parameters Operating parameters Fiscal parameters	$\uparrow$ Performance $\downarrow X_D$ $\downarrow C_{total}$

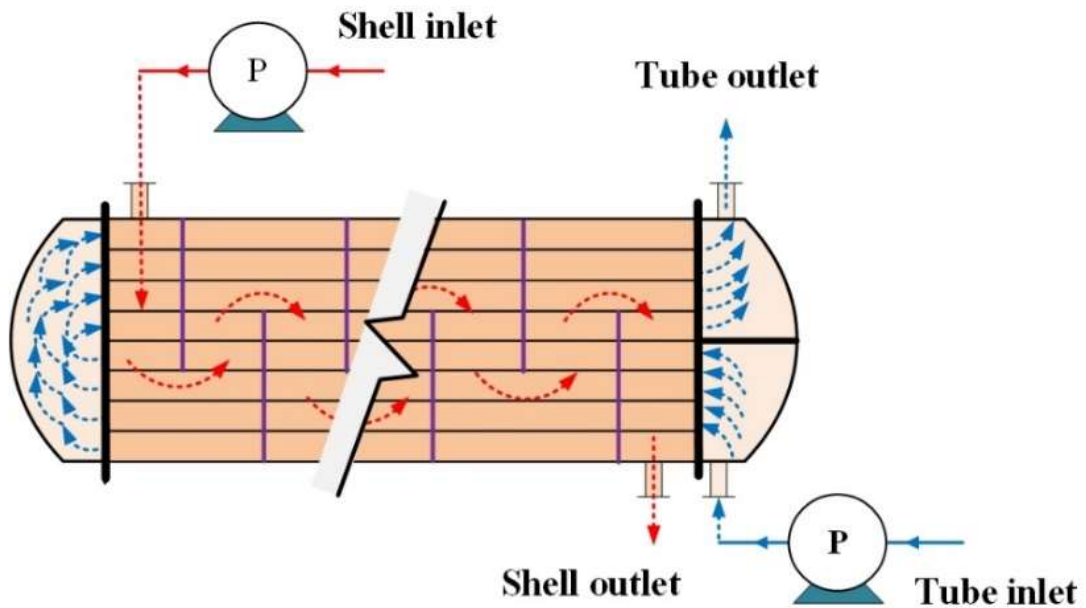
97  $\downarrow$ : Decrease,  $\uparrow$ : Increase



98 **2. System description and methodology**

99 *2.1. Heat exchanger configuration*

100 The system considered in this study consists of a liquid-phase segmental-baffle STHX, which  
101 is used to preheat the water (in the tubes) by transferring heat from the hot stream on the shell-  
102 side, as shown in Figure 1. Two centrifugal pumps are used to maintain the required flow rate and  
103 pressure across the HX. The input data about the process parameters, i.e., fluid inlet-outlet  
104 temperatures and flow rates as well as the geometric parameters, are summarized in Table 2 [49].



105

106 **Figure 1.** Schematic of heat exchanger configuration considered in the current study.

107

108 **Table 2.**  
 109 Specifications of the heat exchanger setup [49].

<b>Parameter</b>	<b>Value</b>
<b><u>Process</u></b>	
Mass flow rate (shell/tube), kg/s	27.80/68.90
Shell side temperature (inlet/outlet), °C	95/40
Tube side temperature (inlet/outlet), °C	25/40
Fouling resistance, $R_f$ (shell/tube), $m^2.K/W$	0.00034/0.00020
<b><u>Geometric</u></b>	
Tube layout, <i>degree</i>	30°
Number of tube passes, $N_p$	2
Length of the tube, $L_t$ , <i>m</i>	4.83
Tube internal diameter, $D_{t,i}$ , <i>m</i>	0.016
Tube external diameter, $D_{t,o}$ , <i>m</i>	0.020
Number of baffles, $N_b$	13
Baffle spacing, $L_{bi}=L_{bo}=L_{bc}$ , <i>m</i>	0.356
Baffle cut, $B_c$ , %	25
Number of pair of sealing strip, $N_{ss}$	2
Diametral shell-to-baffle clearance, $L_{sb}$ , <i>m</i>	0.0051
Diametral tube-to-baffle clearance, $L_{tb}$ , <i>m</i>	0.0008
Baffle thickness, $t_b$ , <i>m</i>	0.005
Tube pitch, $L_{tp}$ , <i>m</i>	0.025
Bypass channel diametral gap, $L_{bb}$ , <i>m</i>	0.019
Shell diameter, $D_s$ , <i>m</i>	0.894
Number of the tube, $N_t$	918
Allowable operating pressure of tube side, $P_t$ , <i>kPa</i>	100
Allowable operating pressure of shell side, $P_s$ , <i>kPa</i>	100

110

111

112 2.2. Thermal-hydraulic design

113 This includes the calculation of tube and shell-side heat transfer coefficients ( $h_t$  and  $h_s$ ),  
114 pressure drops ( $\Delta P_t$  and  $\Delta P_s$ ), overall heat transfer coefficient ( $U$ ), and pumping power. For this  
115 purpose, the Nusselt number ( $Nu$ ) and friction factors ( $f$ ) are calculated for both sides. The tube-  
116 side calculations are straightforward; however, the shell-side calculations constitute a complex  
117 mechanism because of several leakages, inaccuracies, and non-ideal flow streams, etc. Therefore,  
118 the shell-side calculations for thermal-hydraulic performance are conducted using subsequent  
119 approaches:

120 2.2.1. Kern method

121 Kern is the simplest method commonly used for the preliminary design of STHXs [4]. It is  
122 based on the simplest case in STHX that neglects the presence of baffles. In this case, the flow is  
123 across the tubes, and the heat transfer coefficient is similar to a concentric tube heat exchanger,  
124 which could be calculated using equivalent diameter. Nevertheless, in actual practice, the baffles  
125 significantly increase the  $h_s$  as well as  $\Delta P_s$  due to turbulence. Moreover, the fluid velocity varies  
126 because of the confined areas between the tubes across the tube bundle. Therefore, the correlations  
127 for flow inside tubes are not appropriate for shell-side calculations. McAdams [50] proposed  
128 formulation for the calculation of  $h_s$  as:

$$Nu = 0.36 Re^{0.55} Pr^{1/3} \phi^{0.14}$$
$$2 \times 10^3 < Re < 1 \times 10^6, \text{ and } Pr > 0.6 \quad (1)$$

130 The  $\Delta P_s$  to fluid friction, apart from the nozzle losses, is estimated as [28].

$$\Delta P_s = \frac{\rho_s v_s^2}{2} f_s \frac{L_t}{L_{bc}} \frac{D_s}{D_e} \quad (2)$$

$$f_s = 2b_o Re_s^{-0.15} \quad (3)$$

133 where  $b_o$  is a constant, which is assumed to be,  $b_o = 0.72$  by Peters and Timmerhaus [51]. This is  
134 valid for  $Re < 40,000$ ; however, the tube-side pressure drop can be estimated as [52]

$$\Delta P_t = \frac{\rho_t v_t^2}{2} \left( \frac{L_t}{D_{t,i}} f_t + p_c \right) N_p \quad (4)$$

$$f_t = (1.82 \log_{10} Re_t - 1.64)^{-2} \quad (5)$$

137 The value of constant,  $p_c$  is also reported in the literature [49,52], which varies between 2.5 and 4  
 138 by these investigators.

### 139 2.2.2. Bell-Delaware method

140 It is the most accurate method for the design and analysis of STHXs as it acknowledges that  
 141 there is only a portion of the fluid, which is over the tubes in a genuinely cross-flow  
 142 arrangement [9]. The leftover fluid passes through the bypass areas because of the least resistance  
 143 and constitutes up to 40% of the overall flow. Therefore, it is essential to consider the effects of  
 144 non-ideal flow streams while performing thermal-hydraulic calculations [9]. For this purpose, the  
 145 total flow is divided into several streams, i.e., tube hole leakage stream, cross-flow stream, the tube  
 146 bundle bypass stream, the shell-to-baffle bypass stream, and the pass partition bypass stream.  
 147 Therefore,  $h_s$ , is obtained as a product of the ideal cross-flow heat transfer coefficient,  $h_c$ , by the  
 148 correction factors for the non-ideal cross-flow [9].

$$149 \quad h_s = h_c J_C J_L J_B J_S J_R J_\mu \quad (6)$$

150 The ideal cross-flow heat-transfer coefficient ( $h_c$ ) is calculated as [9],

$$151 \quad h_c = j_i c_p G \text{Pr}^{-2/3} \quad (7)$$

$$152 \quad j_i = a_1 \left( \frac{1.33}{L_{tp} / D_t} \right)^a \text{Re}^{a_2} \quad (8)$$

$$153 \quad a = \frac{a_3}{1 + 0.14 \text{Re}^{a_4}} \quad (9)$$

154 where Re is based on tube diameter. The significance and correlations for the calculation of  
 155 correction factors ( $J_s$ ) in Eq. 6 as well as the values of  $a_1$ ,  $a_2$ ,  $a_3$ , and  $a_4$  are given in Appendix A.

156 Similar to the heat transfer coefficient, the shell-side pressure drop is also calculated in three  
 157 parts, i.e., the pressure drop in the central baffle spaces ( $\Delta P_c$ ), baffle windows ( $\Delta P_w$ ), entrance and  
 158 exit baffle spaces ( $\Delta P_e$ ) [9].

$$159 \quad \Delta P_f = \Delta P_c + \Delta P_w + \Delta P_e \quad (10)$$

160 These pressure drops are calculated using the correlation presented in Table 3.

161

162 **Table 3.**  
163 Pressure drop correlations for the Bell-Delaware method [9].

Pressure drop	Governing equation
$\Delta P_c$	$\Delta P_c = \Delta P_{bl} (N_b - 1) R_B R_L, \Delta P_{bl} = 0.002 f_I N_{icc} \frac{G^2}{\rho} R_\mu$ $f_I = b_1 \left( \frac{1.33}{L_{tp} / D_t} \right)^b \text{Re}^{b_2}, b = \frac{b_3}{1 + 0.14 \text{Re}^{b_4}}, R_B = \exp \left[ -C_{bp} F_{sbp} \left( 1 - \sqrt[3]{2r_{ss}} \right) \right]$ $R_L = \exp \left[ -1.33(1 + r_s) r_{lm}^p \right], p = -0.15(1 + r_s) + 0.8, R_\mu = \left( \frac{\mu}{\mu_{wall}} \right)^{-m}$
$\Delta P_w$	$\Delta P_{w, \text{Turbulant}} = N_b \left[ (2 + 0.6 N_{tcw}) \frac{0.001 G_w^2}{2\rho} \right] R_L R_\mu$ $\Delta P_{w, \text{Laminar}} = N_b \left\{ 26 \left( \frac{G_w \mu}{\rho} \right) \left[ \frac{N_{tcw}}{L_{tp} - D_t} + \frac{L_{bc}}{D_w^2} \right] + \left[ \frac{0.002 G_w^2}{2\rho} \right] \right\} R_L R_\mu$ $G_w = \frac{\dot{m}}{\sqrt{S_m S_w}}, D_w = \frac{4S_w}{\pi D_t N_{tw} + (\pi D_s \theta_{ds} / 360)}$ $S_w = \frac{\pi D_s^2}{4} \left( \frac{\theta_{ds}}{360} - \frac{\sin \theta_{ds}}{2\pi} \right) - N_{tw} \left( \frac{\pi}{4} D_t^2 \right)$
$\Delta P_e$	$\Delta P_e = \Delta P_{bl} \left( 1 + \frac{N_{tcw}}{N_{icc}} \right) R_B R_s,$ $R_s = \left( \frac{L_{bc}}{L_{bo}} \right)^{2-n} + \left( \frac{L_{bc}}{L_{bi}} \right)^{2-n}$

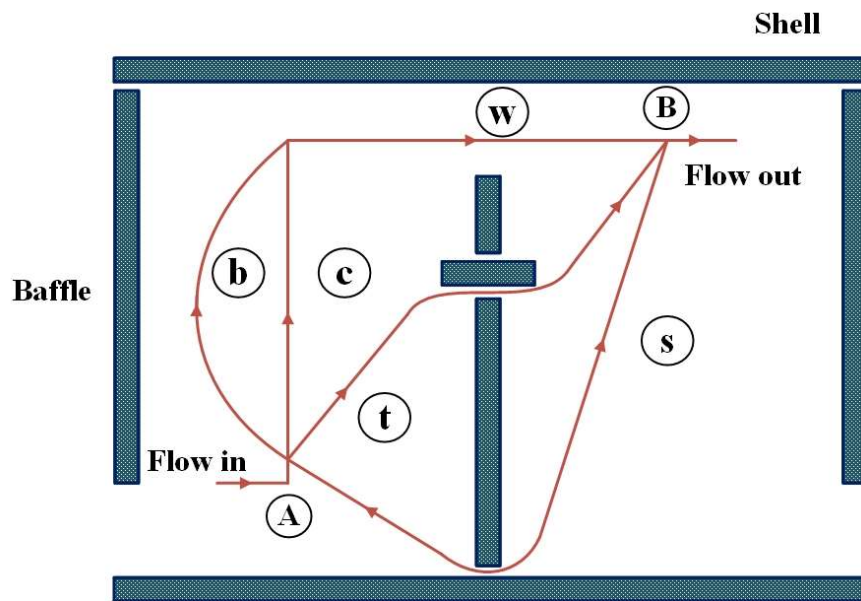
164

165 In the above equations  $\Delta P_{bl}$ : ideal bundle pressure drop for one baffle compartment,  $f_I$ : friction  
166 factor,  $b_1$ - $b_4$ : constants in Table A.1,  $R_B$ : bypass correction factor,  $R_L$ : leakage correction factor,  
167  $R_\mu$ : viscosity correction factor,  $D_w$ : hydraulic diameter,  $S_w$ : window area  $R_B$ : bypass correction  
168 factor,

### 169 2.2.3. Flow stream-analysis method

170 This method calculates the flow rates and pressure drops using a fundamental hydraulic  
171 model that was proposed by Wills-Johnston [4] as a simplified version of Palen and Taborek [53]  
172 work. For this purpose, the flow in the shell-side is divided into various streams as cross-flow,  
173 leakages, and bypass, as illustrated in Figure 2. The flow adopts different paths when moving from

174 A to B. These paths are specified by a subscript. For instance, the flow termed as “leakage” takes  
 175 place between the tubes and baffles (t) and between the baffle and shell. Some of the flow passes  
 176 over the tubes in a cross-flow (c), and part bypasses the tube bundle (b). The cross-flow and  
 177 bypasses streams combine to form a combined window stream (w), which passes through the  
 178 window zone. The shell side heat transfer coefficient is calculated using the actual cross-flow rate  
 179  $\dot{m}_{cross}$  rather than the total shell-side flow rate,  $\dot{m}_S$  as given in Eq. 11-13 [4].



180

181

**Figure 2.** Equivalent shell-side flow [13].

182

$$Nu = 0.211Re^{0.651} Pr^{0.34} \phi^{0.14} \quad (11)$$

183

$$Re = \frac{\dot{m}_{cross} D_t}{\mu S_m} \quad (12)$$

184

where  $S_m$  is the cross-flow area, which is presented in Appendix A.

185

$$\dot{m}_{cross} = F_{cr} \dot{m}_S \quad (13)$$

186

Here  $F_{cr}$  is the portion of flow over the tube bundle in a cross-flow, which is calculated as.

187

$$F_{cr} = \frac{\left(\frac{n_p}{n_a}\right)^{0.5}}{\left(1 + \left(\frac{n_c}{n_b}\right)^{0.5}\right)} \quad (14)$$

188 For calculation of pressure drop, the  $\Delta P$  between two points is taken the same irrespective of  
 189 paths joining these points. The  $\Delta P$  for all the streams is calculated in terms of the coefficient  $n_i$  and  
 190 the respective mass flow rate  $\dot{m}_i$  as

$$191 \quad \Delta P_i = n_i \dot{m}_i^2 \quad (15)$$

192 The total shell side  $\Delta P$  neglecting the inlet and exit nozzles are calculated as.

$$193 \quad \Delta P = n_p \dot{m}^2 (N_b + 1) \quad (16)$$

194 where,  $n$  represent the flow coefficients, which are constant, independent of flow rate, and is a  
 195 function of geometry. The details regarding the calculation of flow coefficients are summarized in  
 196 Appendix A.

### 197 2.3. Exergy analysis

198 Exergy is the maximum theoretical useful work that can be obtained from a system as it is  
 199 brought into a complete thermodynamic equilibrium with the dead state [54]. The specific exergy  
 200 of a fluid stream with negligible kinetic and potential energies is calculated as,

$$201 \quad \bar{ex} = [(h' - h'_0) - T_0(s - s_0)] + \bar{ex}_{che} \quad (17)$$

202 In the above equation  $\bar{ex}_{che}$  represents the specific chemical exergy and has a non-zero value for  
 203 streams with chemical potential such as brackish water, seawater, and brines [55–58].

204 The total exergy in “kW” of each stream is then calculated using the respective flow rate.

$$205 \quad X = \dot{m} \bar{ex} \quad (18)$$

206 Finally, the exergy destruction in the pumps and heat exchanger is estimated by applying  
 207 exergy balance equations. This gives,

$$208 \quad X_{D,STHX} = X_{c,i} + X_{h,i} - X_{c,o} - X_{h,o} \quad (19)$$

$$209 \quad X_{D,P} = X_{w,i} + \dot{W}_{P,i} - X_{w,o} \quad (20)$$

### 210 2.4. Economic analysis

211 This analysis involves the calculation of total cost ( $C_{total}$ ) as a sum of capital cost (CAPC) and  
 212 operating cost (OPC) i.e.,  $C_{total} = CAPC + OPC$ . Conventionally, the CAPC is taken for heat  
 213 exchangers only because of major share (compared to pumps) and the OPC is calculated using  
 214 pumping power [28,37,47]. However, the current study covers exergoeconomic analysis as well,  
 215 which calculates the stream cost using the costs of the heat exchanger as well as the pumps. The

216 details regarding the calculation of different steps involved in the economic analysis are discussed  
 217 in the following sub-sections.

#### 218 2.4.1. Capital cost

219 It reflects the component's purchasing cost and can be obtained through a market survey or  
 220 supplier's quotations. However, the cost obtained by this method cannot accommodate design  
 221 variations. It is, thus, limited for the specified case. Therefore, researchers have developed  
 222 empirical correlations that can satisfactorily approximate the equipment cost based on the major  
 223 design parameters like flow rates, heat transfer area, efficiency, pressure, and temperatures [59].

224 The capital cost of the centrifugal pumps in the current study is calculated using one of the  
 225 most frequently reported correlations [60].

$$226 \quad CAPC_{Pump} = 13.92 \dot{m}_w \Delta P^{0.55} \left( \frac{\eta}{1-\eta} \right)^{1.05} \quad (21)$$

227 The calculation of the capital cost of STHX has been widely discussed because of its extensive  
 228 use under different operating scenarios with varying thermal, hydraulic, and material bounds. In  
 229 this reference, Shabani [61] proposed correlations that relate the capital cost with the weight of  
 230 STHX as given in Eq. 22. Because the weight is not a true measure of heat exchange capacity,  
 231 these correlations are rarely used in the literature.

$$232 \quad CAPC = \exp \left[ x_1 + x_2 \ln(W) \right] \quad (22)$$

233 where  $W$  is the weight in kg, and  $x_1$  and  $x_2$  are constants whose values are available in the  
 234 literature [61].

235 Because of the heat transfer area ( $A$ ) is an accurate indicator of STHX size and capacity, several  
 236 correlations have been developed as a function of the area. In this regard, Turton et al. [62]  
 237 provided a costing correlation for carbon steel (CS) STHX operating at ambient pressure of the  
 238 form.

$$239 \quad \log_{10} CAPC_{amb} = K_1 + K_2 \log_{10} A + K_3 (\log_{10} A)^2 \quad (23)$$

240 However, STHX with higher operating pressures and different construction materials, some  
 241 additional constants and correction factors are multiplied with the base equation. This takes the  
 242 form.

$$243 \quad CAPC = CAPC_{amb} (B_1 + B_2 F_M F_P) \quad (24)$$



244 where  $F_M$  and  $F_P$  are the material and pressure correction factors,  $B_1$  and  $B_2$  are constants. These  
 245 correlations have been used for the optimization of Organic Rankine Cycle STHX [25,63–65].

246 The most reliable and frequently used correlations for CAPC of STHX are those proposed by  
 247 Hall et al. [66] and Taal et al. [67] using simple power law. The general form of these correlations  
 248 is given as.

$$249 \quad \text{CAPC} = x + yA^z \quad (25)$$

250 where  $A$  is the heat transfer area in  $\text{m}^2$  and  $x$ ,  $y$ ,  $z$  are constants which depend on the material of  
 251 tubes and shell. Table 4 summarizes some of the useful correlations for CAPC of STHX.

252 **Table 4.**

253 Correlations for calculation of capital cost (CAPC) of the heat transfer equipment.

Correlation	Material (S/t)	Ref.
$\text{CAPC}^{\$} = 30800 + 750A^{0.81}$	CS-CS	[66]
$\text{CAPC}^{\$} = 30800 + 1339A^{0.81}$	CS-SS	[66]
$\text{CAPC}^{\$} = 30800 + 1644A^{0.81}$	SS-SS	[66]
$\text{CAPC}^{\$} = 7000 + 360A^{0.8}$	CS-CS	[67]
$\text{CAPC}^{\$} = 1000 + 324A^{0.91}$	SS-SS	[67]
$\text{CAPC}^{\$} = 8500 + 409A^{0.85}$	CS-SS	[38,40,42,45,46,67,68]
$\text{CAPC}^{\text{€}} = 8000 + 259.2A^{0.91}$ (✓)	SS-SS	[19,28,30,32– 37,39,43,44,47,67,69]
$\text{CAPC}^{\$} = 10205 + 11.52A$	CS-CS, $A$ ( $\text{ft}^2$ )	[70]
$\log_{10} \text{CAPC}^{\$} = K_1 + K_2 \log_{10} A + K_3 (\log_{10} A)^2$	CS-CS	[25,63–65]
$\text{CAPC}^{\$} = 3.28 \times 10^4 (A/80)^{0.68}$		[71,72]

254 (✓) currently used

255 Caputo et al. [73] critically reviewed these correlations, given all the processes involved in  
 256 STHX manufacturing. They highlighted several limitations of these correlations and proposed a  
 257 very rigorous approach to calculate the STHX cost. The approach involves the calculation of  
 258 material cost as well as the cost of all manufacturing processes like drilling, cutting, beveling,  
 259 chamfering, and welding, which is used to manufacture shells, tube sheets, tube bundles, baffles,  
 260 channels, and flanges, individually. It is comparatively more reliable and flexible for STHX  
 261 optimization, particularly from the manufacturing perspective. However, for performance analysis  
 262 of STHX as a system component, this detailed approach is not computationally economical.

263 Hence, the purchased equipment cost correlations based on the heat transfer area rather than  
 264 manufacturing cost reasonably serve the purpose.

265 Moreover, it is essential to emphasize that the correlations discussed above and used in the  
 266 current study were developed about 30 years back. The cost calculated using these correlations is  
 267 precise only for the time they were developed [73]. Therefore, it is appropriate to improve these  
 268 correlations to recent times using cost indices to accommodate the inflation and variations in the  
 269 market scenarios [25]. For this purpose, the idea of using a cost index factor ( $C_{index}$ ) has been  
 270 adopted [24,65]. The  $C_{index}$  is calculated using the Chemical Engineering Plant Cost Index (CEPCI)  
 271 of the reference year and the current year [63].

$$272 \quad C_{index} = \frac{CEPCI_{current}}{CEPCI_{reference}} \quad (26)$$

273 Thus, the current CAPC of the equipment is given as [64],

$$274 \quad CAPC_{current}^S = C_{index} \times CAPC_{reference}^S \quad (27)$$

275 In the present study, the  $C_{index}$  is calculated to be 1.7 based on the  $CEPCI_{1990} = 390$  [74] and  
 276  $CEPCI_{2020} = 650$  [75]. However, for rigorous design and analysis purposes, the effect of  $C_{index}$  is  
 277 also studied in this paper for a wide range of values.

#### 278 2.4.2. Operational cost

279 The OPC is calculated based on current annual cost  $C_o$  (\$/y), equipment life,  $n_y$  (year), unit  
 280 electricity price,  $C_{elec}$  (\$/kWh), annual inflation rate,  $i$  (%), operational availability  $\Lambda$  (hour), and  
 281 pumping power,  $PP$ , (kW) as.

$$282 \quad OPC = \sum_{j=1}^{n_y} \frac{C_o}{(1+i)^j} \quad (28)$$

$$283 \quad C_o = PP \times C_{elec} \times \Lambda \quad (29)$$

$$284 \quad PP = \left( \frac{\dot{m}_{tube} \Delta p_{tube}}{\rho_{tube}} + \frac{\dot{m}_{shell} \Delta p_{shell}}{\rho_{shell}} \right) \times \frac{1}{\eta} \quad (30)$$

285 In the current case study, the values of fiscal parameters are taken as  $n_y = 10$  year,  $\Lambda = 7000$  h/y,  $i =$   
 286 10%,  $C_{elec} = 0.12$  (\$/kWh) and  $\eta = 70\%$  [28].

287 2.4.3. Exergoeconomic analysis

288 After the calculation of capital and operational cost, the analysis is applied to calculate the  
 289 stream cost [76]. For this purpose, the CAPC calculated above is first converted to the annual rate  
 290 of capital investment  $\dot{Z}$  (\$/y) using the capital recovery factor (CRF) [77]. The CRF is calculated  
 291 based on the interest rate ( $i$ ) and amortization years/economic life of the plant ( $n_y$ ), as given below  
 292 [78]:

$$293 \quad CRF = \frac{i \times (1+i)^{n_y}}{(1+i)^{n_y} - 1} \quad (31)$$

$$294 \quad \dot{Z} = CRF \times CAPC \quad (32)$$

295 Finally, the rate of fixed cost  $\zeta$  (in \$/s) is calculated using the plant availability ( $\Lambda$ ) as [79].

$$296 \quad \zeta = \frac{\dot{Z}}{3600 \times \Lambda} \quad (33)$$

297 After that, a general cost balance equation is applied to each component in the system. This is  
 298 expressed as [80].

$$299 \quad \dot{C}_o = \Sigma \dot{C}_i + \zeta \quad (34)$$

300 where  $\dot{C}_o$  represents the local output stream cost,  $\dot{C}_i$  the cost of the input stream, and  $\zeta$  the rate  
 301 of fixed (purchased equipment) cost.

302 The cost balance equation for the pump and heat exchanger, respectively, are given as:

$$303 \quad \dot{C}_o = \dot{C}_i + C_{elec} \dot{W}_{Pump} + \zeta_{Pump} \quad (35)$$

$$304 \quad \dot{C}_{c,o} = \dot{C}_{c,i} + \dot{C}_{h,i} - \dot{C}_{h,o} + \zeta_{STHX} \quad (36)$$

305 It is important to mention that for the components with multiple outlet streams (i.e., heat  
 306 exchangers, evaporators, flash chambers and membrane modules, etc.), additional auxiliary  
 307 equations are required. For a system with “k” outlet streams, “k-1” number of auxiliary equations  
 308 are required to solve the system [21]. These equations are based on the equality of the inlet and  
 309 outlet streams cost averaged with exergy of the respective streams as given in Eq. 37 [81].

$$310 \quad \frac{\dot{C}_{h,i}}{X_{h,i}} - \frac{\dot{C}_{h,o}}{X_{h,o}} = 0 \quad (37)$$

311 *2.5. Sensitivity analysis*

312 Sensitivity analysis is an important tool to ascertain insight into the significance of model  
 313 parameters and, in turn, identify those, which are more responsive [82]. The results of this analysis  
 314 not only help in improving the system performance but also highlight the important areas for future  
 315 research [83]. Calculus-based sensitivity analysis is one of the most fundamental and reliable  
 316 methods for this purpose. This method models each independent parameter as a sum of its nominal  
 317 value and the perturbation or uncertainty as given below [84].

318 
$$X = \bar{X} \pm \hat{U}_X \quad (38)$$

319 where  $\bar{X}$  is the nominal value and  $\pm\hat{U}_X$  is possible uncertainty about the nominal value. The  
 320 corresponding uncertainty in the response variable  $Y(X)$  due to uncertainty in  $X$  is expressed in a  
 321 differential form as [85],

322 
$$\hat{U}_Y = \frac{dY}{dX} \hat{U}_X \quad (39)$$

323 For a multi-variable function  $Y = Y(X_j, X_{j+1}, \dots, X_N)$ , the uncertainty in  $Y$  due to the  
 324 perturbations in the  $X$  is calculated as the root sum square product of the individual perturbation  
 325 computed to the first-order accuracy, as given in Eq. 40. Each partial derivative in the equation  
 326 represents the sensitivity coefficient (SC), which depicts the sensitivity of output parameters to  
 327 small changes in the respective input parameter [86].

328 
$$\hat{U}_Y = \left[ \sum_{j=1}^N \left( \frac{\partial Y}{\partial X_j} \hat{U}_{X_j} \right)^2 \right]^{1/2} \quad (40)$$

329 Meanwhile, a more convenient and comprehensive way of presenting the findings of sensitivity  
 330 analysis is through Normalized Sensitivity Coefficients (NSC) [87]. It allows the direct (one-on-  
 331 one) comparison of parameters whose order of magnitude could be significantly different [88].  
 332 These NSCs are obtained by normalizing the uncertainties in the response parameter  $Y$  and input  
 333 parameter  $X$  by its respective nominal values. For this, the coefficients in Eq. 40 are transformed  
 334 into NSC and normalized uncertainties (NU) as given by [89].

335 
$$\frac{\hat{U}_Y}{\bar{Y}} = \left[ \sum_{j=1}^N \left( \overbrace{\left( \frac{\partial Y}{\partial X_j} \frac{\bar{X}_j}{\bar{Y}} \right)^2}^{NSC} \right) \left( \overbrace{\left( \frac{\hat{U}_{X_j}}{\bar{X}_j} \right)^2}^{NU_{X_j}} \right) \right]^{1/2} \quad (41)$$

336 In the current study, the sensitivity of input parameters like mass flow rate, inlet-outlet  
 337 temperatures, baffle spacing, and fiscal parameters (interest rate and electricity cost) on the output  
 338 parameters i.e.,  $h$ ,  $\Delta P$ ,  $OPC$ , and  $C_{s,o}$  is studied. The equations developed and used for this analysis  
 339 are given as follows.

$$340 \quad \frac{\hat{U}_{h_s}}{\bar{h}_s} = \left[ \begin{aligned} & \left( \frac{\partial h_s}{\partial \dot{m}_s} \frac{\bar{m}_s}{\bar{h}_s} \right)^2 \left( \frac{\hat{U}_{\dot{m}_s}}{\bar{\dot{m}}_s} \right)^2 + \left( \frac{\partial h_s}{\partial L_{bc}} \frac{\bar{L}_{bc}}{\bar{h}_s} \right)^2 \left( \frac{\hat{U}_{L_{bc}}}{\bar{L}_{bc}} \right)^2 + \left( \frac{\partial h_s}{\partial T_{s,i}} \frac{\bar{T}_{s,i}}{\bar{h}_s} \right)^2 \left( \frac{\hat{U}_{T_{s,i}}}{\bar{T}_{s,i}} \right)^2 \\ & + \left( \frac{\partial h_s}{\partial T_{s,o}} \frac{\bar{T}_{s,o}}{\bar{h}_s} \right)^2 \left( \frac{\hat{U}_{T_{s,o}}}{\bar{T}_{s,o}} \right)^2 \end{aligned} \right]^{1/2} \quad (42)$$

$$341 \quad \frac{\hat{U}_{\Delta P_s}}{\Delta P_s} = \left[ \left( \frac{\partial \Delta P_s}{\partial \dot{m}_s} \frac{\bar{m}_s}{\Delta P_s} \right)^2 \left( \frac{\hat{U}_{\dot{m}_s}}{\bar{\dot{m}}_s} \right)^2 + \left( \frac{\partial \Delta P_s}{\partial L_{bc}} \frac{\bar{L}_{bc}}{\Delta P_s} \right)^2 \left( \frac{\hat{U}_{L_{bc}}}{\bar{L}_{bc}} \right)^2 \right]^{1/2} \quad (43)$$

$$342 \quad \frac{\hat{U}_{OPC}}{OPC} = \left[ \begin{aligned} & \left( \frac{\partial OPC}{\partial \dot{m}_s} \frac{\bar{m}_s}{OPC} \right)^2 \left( \frac{\hat{U}_{\dot{m}_s}}{\bar{\dot{m}}_s} \right)^2 + \left( \frac{\partial OPC}{\partial L_{bc}} \frac{\bar{L}_{bc}}{OPC} \right)^2 \left( \frac{\hat{U}_{L_{bc}}}{\bar{L}_{bc}} \right)^2 + \left( \frac{\partial OPC}{\partial C_{elec}} \frac{\bar{C}_{elec}}{OPC} \right)^2 \left( \frac{\hat{U}_{C_{elec}}}{\bar{C}_{elec}} \right)^2 \\ & + \left( \frac{\partial OPC}{\partial i} \frac{\bar{i}}{OPC} \right)^2 \left( \frac{\hat{U}_i}{\bar{i}} \right)^2 \end{aligned} \right]^{1/2} \quad (44)$$

$$343 \quad \frac{\hat{U}_{C_{s,o}}}{\bar{C}_{s,o}} = \left[ \begin{aligned} & \left( \frac{\partial C_{s,o}}{\partial \dot{m}_s} \frac{\bar{m}_s}{\bar{C}_{s,o}} \right)^2 \left( \frac{\hat{U}_{\dot{m}_s}}{\bar{\dot{m}}_s} \right)^2 + \left( \frac{\partial C_{s,o}}{\partial L_{bc}} \frac{\bar{L}_{bc}}{\bar{C}_{s,o}} \right)^2 \left( \frac{\hat{U}_{L_{bc}}}{\bar{L}_{bc}} \right)^2 + \left( \frac{\partial C_{s,o}}{\partial C_{elec}} \frac{\bar{C}_{elec}}{\bar{C}_{s,o}} \right)^2 \left( \frac{\hat{U}_{C_{elec}}}{\bar{C}_{elec}} \right)^2 \\ & + \left( \frac{\partial C_{s,o}}{\partial i} \frac{\bar{i}}{\bar{C}_{s,o}} \right)^2 \left( \frac{\hat{U}_i}{\bar{i}} \right)^2 \end{aligned} \right]^{1/2} \quad (45)$$

344 Finally, the relative contribution (RC) of each parameter is estimated to identify the dominant  
 345 uncertainty contributors by combining the sensitivity coefficients with the actual uncertainty [88].  
 346 Its mathematical form is obtained as the square of the product of sensitivity coefficient and  
 347 uncertainty, normalized by the square of the uncertainty in the response parameter [89].

$$348 \quad RC = \frac{\left( \frac{\partial Y}{\partial X_j} \hat{U}_{X_j} \right)^2}{\hat{U}_Y^2} \quad (46)$$

349 *2.6. Numerical solution and assumptions*

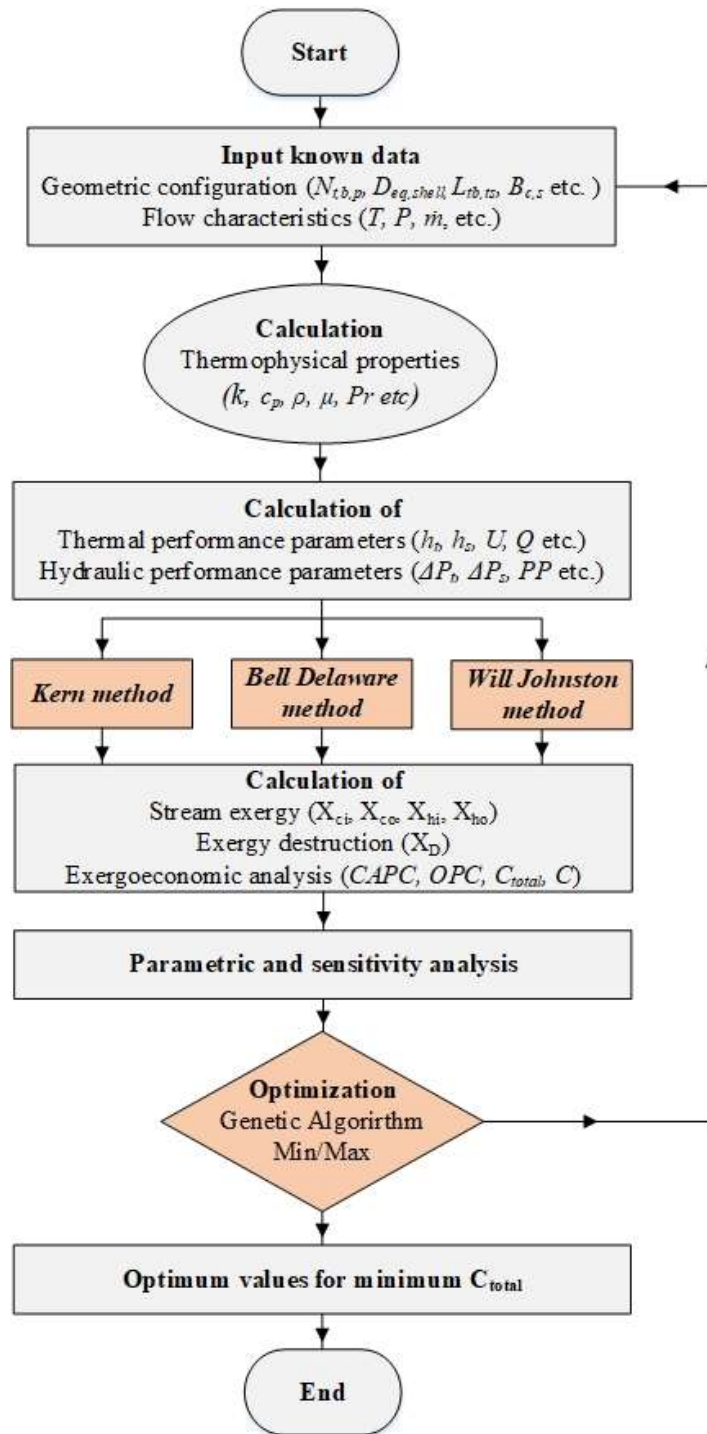
350 The mathematical model discussed above is solved using an Engineering Equation Solver  
351 (EES) based numerical code. In the first step, the input data consisting of flow rates, temperatures,  
352 and geometric parameters are provided. The EES library routines are used to calculate the  
353 thermophysical properties and correction factors for STHX. After that, the code works using  
354 algorithms of the three methods (i.e., Kern, Bell-Delaware, and Wills-Johnston). For the Kern  
355 method, the Nu and  $\Delta P$  are calculated directly using Eq. 1, 2, and 4 which also involve the  
356 calculation of Re, friction factor, equivalent diameter, etc.

357 While, the Bell Delaware method additionally focuses on the calculation of ideal heat transfer  
358 coefficient (given in Eq. 7), ideal pressure drop for baffle compartment, window cross areas,  
359 window tubes. Besides, the method also involves the calculation of correction factors (presented  
360 in Table A.2) i.e., baffle cut, baffle leakage, bundle bypass, un-equal baffle spacing, laminar flow,  
361 and wall viscosity correction factor, etc. These correction factors are used in Eq. 6 and to calculate  
362 the shell side heat transfer coefficient. Similarly, in this method, the total shell side pressure drop  
363 is calculated in three portions i.e., across the tube bundle, in the window zone, and inlet and exit  
364 baffles. These individual pressure drops add up to the total pressure drop given in Eq 10.

365 In the Wills-Johnston method, the parameters like flow fractions and resistances i.e., combined  
366 flow, cross flow, bypass flow, shell side flow, tube side flow, window flow, and end window flow  
367 resistance are determined first using relations presented in Table A.3. Thereafter these are used to  
368 calculate the crossflow rate, Re, Nu, shell side local/overall heat transfer coefficient, and total shell  
369 side pressure drop using Eqs. (11) – (16). The total shell side pressure drop is the sum of the  
370 pressure drop at the central window and the pressure drop at the end window zones.

371 In each case, the numerical code is validated with the literature for all three methods followed  
372 by a comprehensive thermal, hydraulic, exergetic, and exergoeconomic analysis of STHX, as  
373 summarized in Fig. 3. Finally, the genetic algorithm is employed to optimize the heat exchanger  
374 design taking cost as an objective function (for which the working is discussed in detail in  
375 subsequent Section 4.5). The analysis is based on the following assumptions: (a) steady-state  
376 operation, (b) negligible longitudinal conduction, (c) uniform heat transfer coefficients, (d)  
377 negligible heat and pressure losses in the connecting pipes, and (e) no thermal energy source or  
378 sink in the HX or fluid.

379



380

381

Figure 3. Solution flow chart.

### 382 3. Results and discussion

#### 383 3.1. Numerical model validation

384 The EES-based numerical code was developed to solve the governing equations of Kern,  
385 Bell-Delaware, and Wills-Johnston's methods, in addition to validation with the literature, as  
386 presented in Table 5. The first two methods are validated with the case discussed by Sinnott and  
387 Towler [49], which is recently used by Caputo et al. [28] and Sadeghzadeh et al. [37]. The case is  
388 based on a methanol-to-brackish water heat exchanger with a triangular pitch and a heat duty of  
389 4.34 MW with one shell and two-tube-side passes. The inlet and out temperatures and flow rates  
390 are as follows  $T_{S,i} = 95^{\circ}C$ ,  $T_{t,i} = 25^{\circ}C$ ,  $T_{S,o} = 40^{\circ}C$ ,  $T_{t,o} = 40^{\circ}C$ ,  $\dot{m}_s = 27.80$  kg/s, and  
391  $\dot{m}_t = 68.90$  kg/s. While the third method (i.e., Wills-Johnston) is validated with the case presented  
392 by Serth [90]. It involves kerosene-to- crude oil heat exchanger with a heat duty of 1.089 MW,  
393 one shell- and four tube-side passes. The process parameters used are  $T_{S,i} = 390^{\circ}F$ ,  $T_{t,i} = 100^{\circ}F$   
394 ,  $T_{S,o} = 250^{\circ}F$ ,  $T_{t,o} = 150^{\circ}F$ ,  $\dot{m}_s = 45000$  lb/h, and  $\dot{m}_t = 150,000$  lb/h.

395 The results showed a reasonable agreement between the values obtained by the current  
396 analysis and literature values. However, a remarkable deviation ( $\pm 12$  %) is observed in the shell-  
397 side heat transfer coefficient calculated by using the Kern method. This is presumably because of  
398 the empirical heat transfer correlation that does not consider various leakages and baffle  
399 configurations in the Kern method, while the other two methods consider all the possible effects  
400 in developing the heat transfer and pressure drop correlations. It is important to note that the  
401 remaining results are satisfactorily close to the values reported in the literature for all the cases.

402

403



404 **Table 5.**

405 Validation of Kern and Bell Delaware and Wills Johnston methods numerical code.

Parameters	Values		
	Literature [28,37,49]	Present work	Error %
$A, m^2$	278.6	278.6	0 %
$Q (MJ)$	4.34	4.34	0 %
$S_s, m^2$	0.06365	0.06365	0%
$h_t, W/m^2k$	3812	3811	$\pm 0.026$ %
$\Delta P_t, Pa$	6251	6166	$\pm 1.35$ %
$C_{total}, \epsilon$	64,480	64,266	$\pm 0.331$ %
<b>Kern method</b>			
$Re$	18,381	18,572	$\pm 1.039$ %
$h_s, W/m^2k$	1573	1791*	$\pm 12.171$ %
$\Delta P_s, Pa$	35,789	35,166	$\pm 1.740$ %
<b>Bell-Delaware method</b>			
$Re$	26,353	24,176	$\pm 8.260$ %
$h_s, W/m^2k$	1246	1159	$\pm 6.982$ %
$\Delta P_s, Pa$	8050	8054	$\pm 0.049$ %
<b>Wills-Johnston method [90]</b>			
$S_b, ft^2$	0.03583	0.03583	$\pm 0$ %
$F_{cr}$	0.345	0.345	$\pm 0$ %
$Re$	10,569	10,531	$\pm 0.359$ %
$h_s, btu/h. ft^2F$	----	177.6	----
$\Delta P_s, psi$	1.25	1.27	$\pm 1.6$ %

406 \*: major difference, ----: Not available

407

408 3.2. *Heat exchanger design*

409 The above validated numerical code is employed to design a liquid-phase water-water STHX  
410 using Kern, Bell-Delaware, and Wills-Johnston methods. The process and geometric parameters  
411 used as input data are summarized in Table 2. The output parameters, including heat transfer  
412 coefficients, pressure drops, pumping power, exergy destruction, capital, operational, and stream  
413 costs, are calculated and presented in Table 6. It also presents a rationale comparison of two  
414 commonly used (i.e., Kern and Bell-Delaware) and one rarely adopted (i.e., Wills-Johnston) STHX  
415 design methods from thermal, hydraulic, exergetic, and economic viewpoints. It is observed that;  
416 the Kern method shows a significant over/underestimation of shell-side parameters compared to  
417 Bell-Delaware (which is known to be the most accurate STHX design method). For instance, the  
418 shell-side heat transfer coefficient, pressure drop, pumping power, operational and total costs  
419 calculated using the Kern method deviates from those calculated using Bell-Delaware by  $\pm 56\%$ ,  
420  $\pm 330\%$ ,  $\pm 100\%$ ,  $\pm 100\%$ , and  $\pm 4.85\%$ , respectively; however, for Wills-Johnston, these deviations  
421 are significantly lower with  $\pm 7.4\%$ ,  $\pm 49\%$ ,  $\pm 15\%$ ,  $\pm 15\%$ , and  $\pm 0.8\%$ , respectively.

422 It is important to mention that the large-scale deviations in the Kern method are primarily  
423 because it ignores the effect of baffles and associated leakages on the shell-side flow. While the  
424 other two methods accommodate the presence of baffles through correction factors and flow  
425 coefficients. Therefore, it is reasonable to assert that the reliability of the design and analysis of  
426 STHX conducted is the highest for Bell-Delaware followed by Wills-Johnston and then Kern  
427 method. Particularly, from a monetary viewpoint, the Kern method is only suitable for preliminary  
428 sizing, however, for a satisfactory design, the other two methods should be preferred to reduce  
429 capital and operation investments associated with the over and underestimations.

430

431 **Table 6.**

432 A preliminary design with three methods i.e., Kern, Bell-Delaware, and Wills-Johnston.

Parameter	Case study: Water to Water STHX		
	Kern	Bell-Delaware	Wills-Johnston
$A, m^2$	■ 278.6	278.6	278.6 ■
$Re_t$	■ 15,779	15,779	15,779 ■
$h_t, W/m^2K$	■ 4053	4053	4053 ■
$Re_s$	▼ 15,095	19,621	4281* ▼
$h_s, W/m^2K$	▲ 4300	2748	2952 ▲
$U, W/m^2K$	▲ 854	768	785 ▲
$\Delta P_t, Pa$	■ 6098	6098	6098 ■
$\Delta P_s, Pa$	▲ 27,786	6447	3257 ▼
$h_s/\Delta P_s, m/s K$	▼ 0.1548	0.4262	0.9065 ▲
$PP, kW$	▲ 1.73	0.8648	0.7354 ▼
$X_{D\ Total}, kW$	▲ 685	684	684 ▼
$CAPC_{HX}, \text{€}$	■ 87,562	87,562	87,562 ■
$CAPC_{total}, \text{€}$	▲ 89,589	88,936	88,751 ▼
$\dot{Z}_{total}, \text{€}/h$	▲ 2.083	2.068	2.064 ▼
$OPC, \text{€}$	▲ 8931	4464	3796 ▼
$C_{total}, \text{€}$	▲ 96,492	92,025	91,357 ▼
$\dot{C}_{c,o}, \text{€}/h$	▲ 2.282	2.169	2.151 ▼
$\dot{C}_{h,o}, \text{€}/h$	▲ 0.00845	0.00227	0.00126 ▼

433 ▲: Overestimation, ▼: Underestimation, ■: Same

434 \* The major difference is because of cross-flow which is merely 0.3 to 0.5 of the total flow

435 3.3. Sensitivity analysis

436 The sensitivity analysis outcomes in the form of Normalized Sensitivity Coefficients (NSC)  
437 and Relative Contribution (RC) for the Bell-Delaware method are summarized in Figure 4 (a)  
438 to (d). The results are presented for critical input parameters (for which  $NSC \geq 0.0001$ ). Figure 4  
439 (a) highlights the input parameters that have an impact on the shell-side heat transfer coefficient.  
440 It shows that for the given case, the most critical parameters in terms of NSC are shell-side flow  
441 rate  $\dot{m}_s$ , followed by shell inlet temperature  $T_{S,i}$ , central baffle spacing  $L_{bc}$ , and shell outlet  
442 temperature  $T_{S,o}$ , respectively. While, the RC is dominated by the uncertainty in  $\dot{m}_s$  with 98%  
443 followed by  $L_{bc}$ ,  $T_{S,i}$ , and  $T_{S,o}$ , with 2%, 0.11%, and 0.10%, respectively.

444 Similarly, Figure 4 (b) shows that the shell-side pressure drop ( $\Delta P_S$ ) is the most sensitive to  
445 the  $L_{bc}$  followed by  $\dot{m}_s$ . However, the relative contribution is higher  $\sim 76\%$  for  $\dot{m}_s$  and lower for  $L_{bc}$   
446 with  $\sim 23\%$  and almost insignificant for inlet and outlet temperatures. The operational cost displays  
447 (refer Figure 4 (c)) the highest NSC for unit electricity cost ( $C_{elec}$ ) with  $\sim 1$ , followed by  $\dot{m}_s$  with  
448  $\sim 0.78$ ,  $L_{bc}$  with  $\sim 0.4$ , and interest rate ( $i$ ) with  $\sim 0.2$ , respectively. The corresponding RC values are  
449 65%, 20%, 9%, and 3%, respectively. Concurrently, the stream cost shows (see Figure 4 (d)) the  
450 highest NSC for  $\dot{m}_s$ , followed by  $L_{bc}$ ,  $C_{elec}$ , and  $i$ , respectively. The RC values are calculated as  $\sim$   
451 86% for  $\dot{m}_s$ ,  $\sim 11\%$  for  $L_{bc}$ ,  $\sim 1.8\%$  for  $C_{elec}$ , and  $\sim 0.05\%$  for  $i$ .

452 The findings of the sensitivity analysis infer that the thermal-hydraulic performance (i.e.,  $h$  and  
453  $\Delta P$ ) of STHXs is sensitive to the flow characteristics, and the economic performance is equally  
454 governed by the fiscal parameters such as unit electricity cost and interest rate. Therefore, a  
455 commensurate importance should be apportioned to the fiscal parameters while conducting the  
456 economic analysis of heat exchangers. It is also important to emphasize that the discrepancies  
457 between maximum NSC and RC values for dissimilar parameters are well explained by James et  
458 al. [88]. This is because the small uncertainties associated with the highest sensitivity coefficients  
459 shift the relative contribution toward the input parameters with lower-sensitivity coefficients,  
460 especially those with high uncertainties. Moreover, it is also worth mentioning that one order of  
461 magnitude alteration (as adopted in the sensitivity analysis) is usually not of practical interest,  
462 rather it should be perceived only as a limiting case to obtain directly comparable values.

463

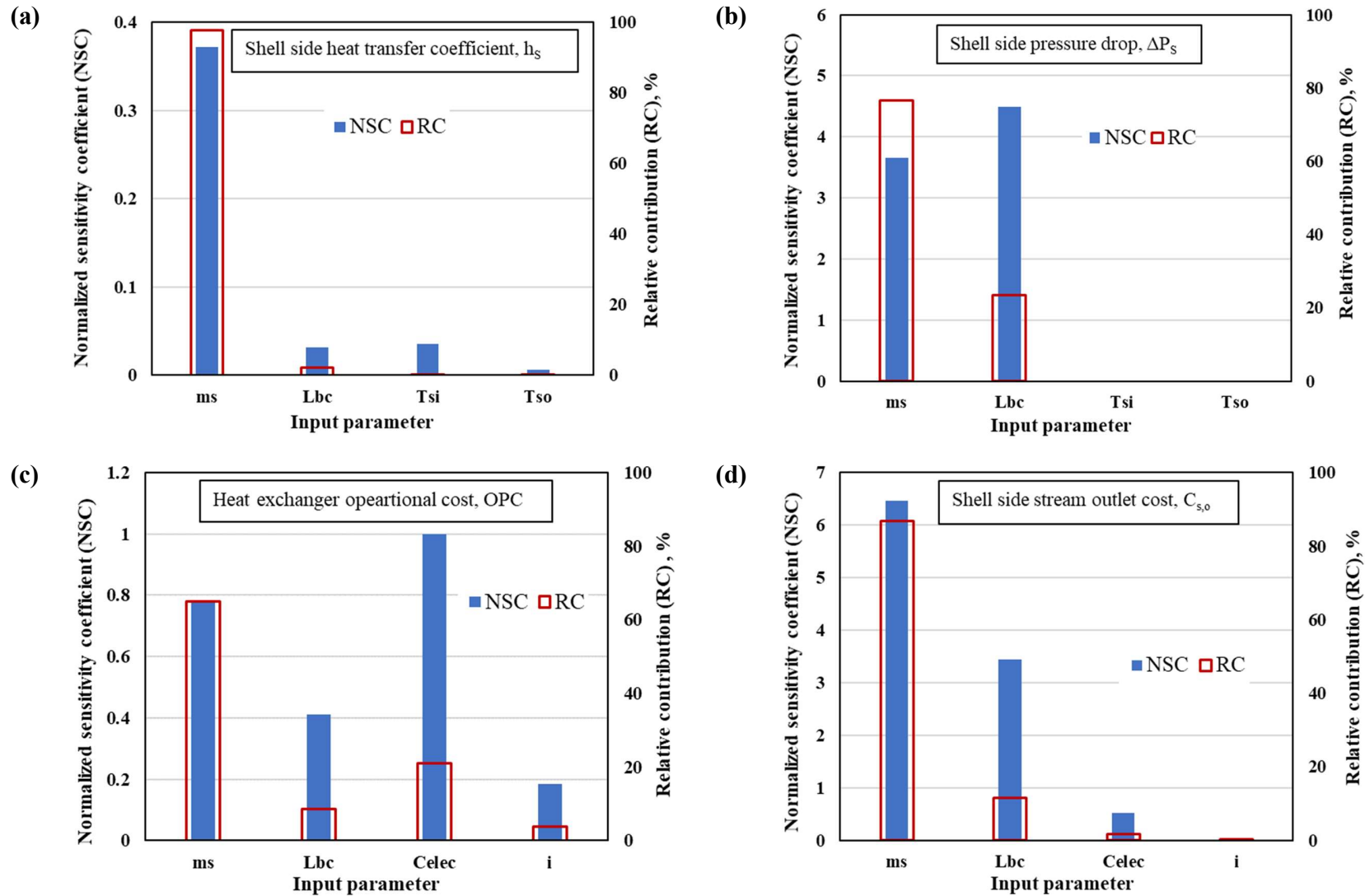


**Figure 4.** Sensitivity analysis results, i.e., NSC and RC of different input parameters on performance parameters (a)  $h_s$ , (b)  $\Delta P_s$ , (c)  $OPC$ , and (d)  $C_{o,s}$ .

464

465

466 3.4. Parametric analysis

467 A detailed parametric analysis is conducted using the one-factor-at-a-time (OFAT) approach  
468 to investigate the real scale effect of important input parameters on the thermal, hydraulic, and  
469 economic performance of STHX. The results are presented combinedly for Kern, Bell-Delaware,  
470 and Wills-Johnston methods, which illustrate the deviation of three methods (from each other)  
471 over a range of operating conditions.

472 3.4.1. Effect of shell-side flow rate

473 The mass flow rate is one of the most influential process parameters (as indicated by the  
474 sensitivity analysis) that governs the thermal, hydraulic, and economic performance of heat  
475 exchangers. It is observed that an increase in shell-side flow-rate increased the heat transfer  
476 coefficient ( $h_s$ ); however, the corresponding pressure drop ( $\Delta P$ ) also increased as shown in  
477 Figure 5 (a) and (b). This is because the higher flow rate resulted in a higher shell-side Reynolds  
478 number, which intensified the turbulence that controls the heat transfer rate and pressure drops.  
479 Hence, there should be a tradeoff between the heat transfer coefficient and pressure drop for  
480 optimal performance. In this regard, the heat transfer coefficient per unit pressure drop ( $h/\Delta P$ )  
481 gives a reasonable estimation of the overall thermal-hydraulic performance of heat exchangers.  
482 From Figure 5 (c), it is seen that an increase in shell-side flow rate decreased the  $h/\Delta P$  showing a  
483 higher-order rise in the pressure drop compared to the heat transfer capability. However, up to 15-  
484 20 kg/s, the  $h/\Delta P$  is well above unity showing higher heat transfer than pressure drops.

485 Similarly, an increase in the shell-side flow rate increased the operating and stream (product)  
486 cost as shown in Figure 6. For instance, the operational cost calculated using Bell-Delaware and  
487 Wills-Johnston methods varied from ~3,000 to 10,000 € for flow rate varying from 1 to 50 kg/s.  
488 While for the Kern method, it approached ~34,000 € for the same flow rate variations, which  
489 indicate the overestimation of hydraulic and economic parameters and the limitations of the Kern  
490 method at higher flow rates. Likewise, the cold water outlet stream cost approached 2.3 €/h for  
491 Bell-Delaware and Wills-Johnston methods, while above 2.8 €/h for the Kern method. A similar  
492 trend is observed for the hot water outlet stream with different magnitudes (varying between 0.005  
493 to 0.01 €/h for Bell-Delaware and Wills-Johnston methods, and 0.040 €/h for the Kern method.  
494 From these observations, it is reasonable to assert that the Kern method gives a very rough estimate  
495 regarding the heat exchanger design, particularly at high flow rates. Hence, for a practical design,  
496 the other two methods should be preferred to minimize energy and monetary investments.

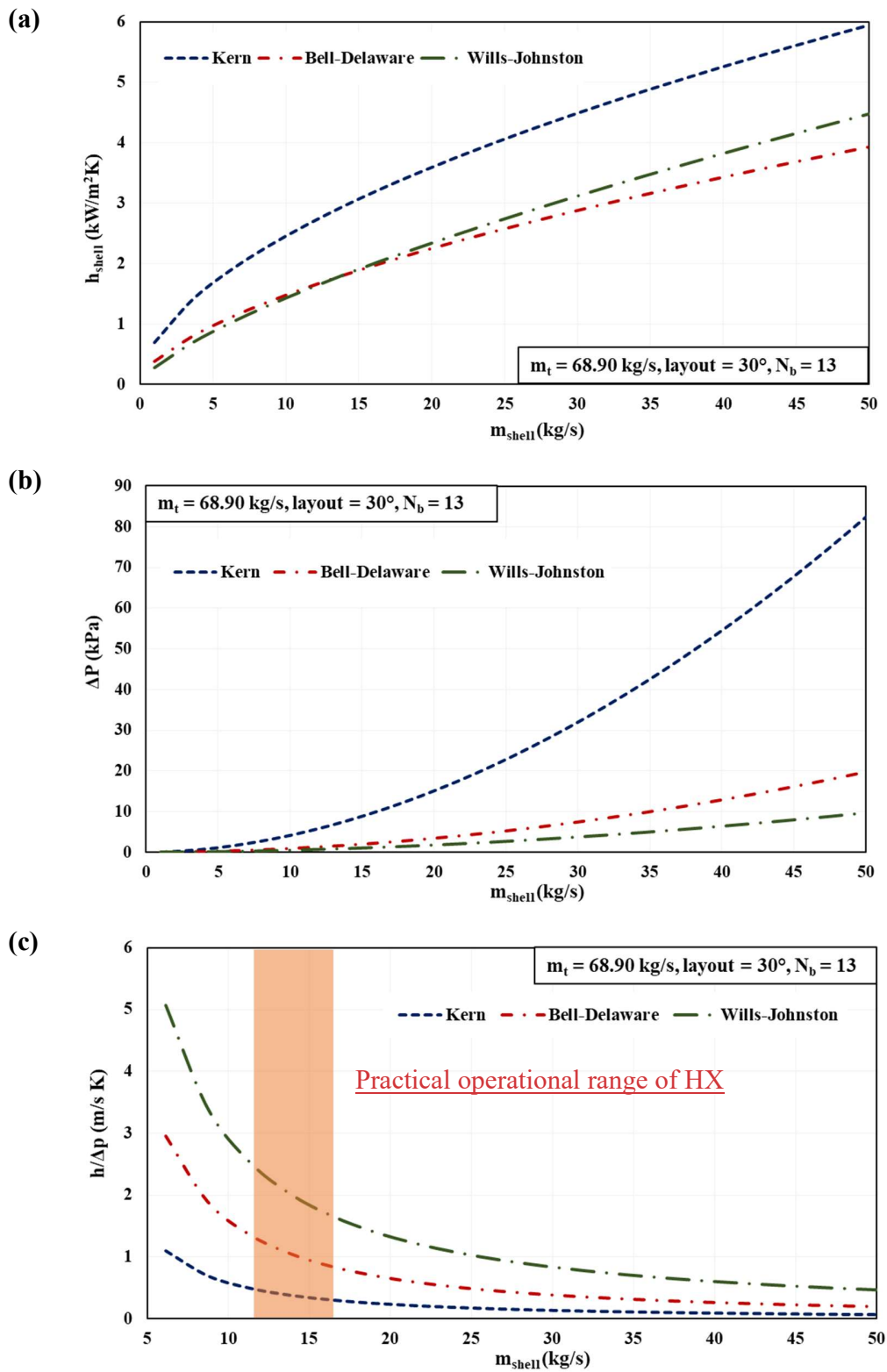
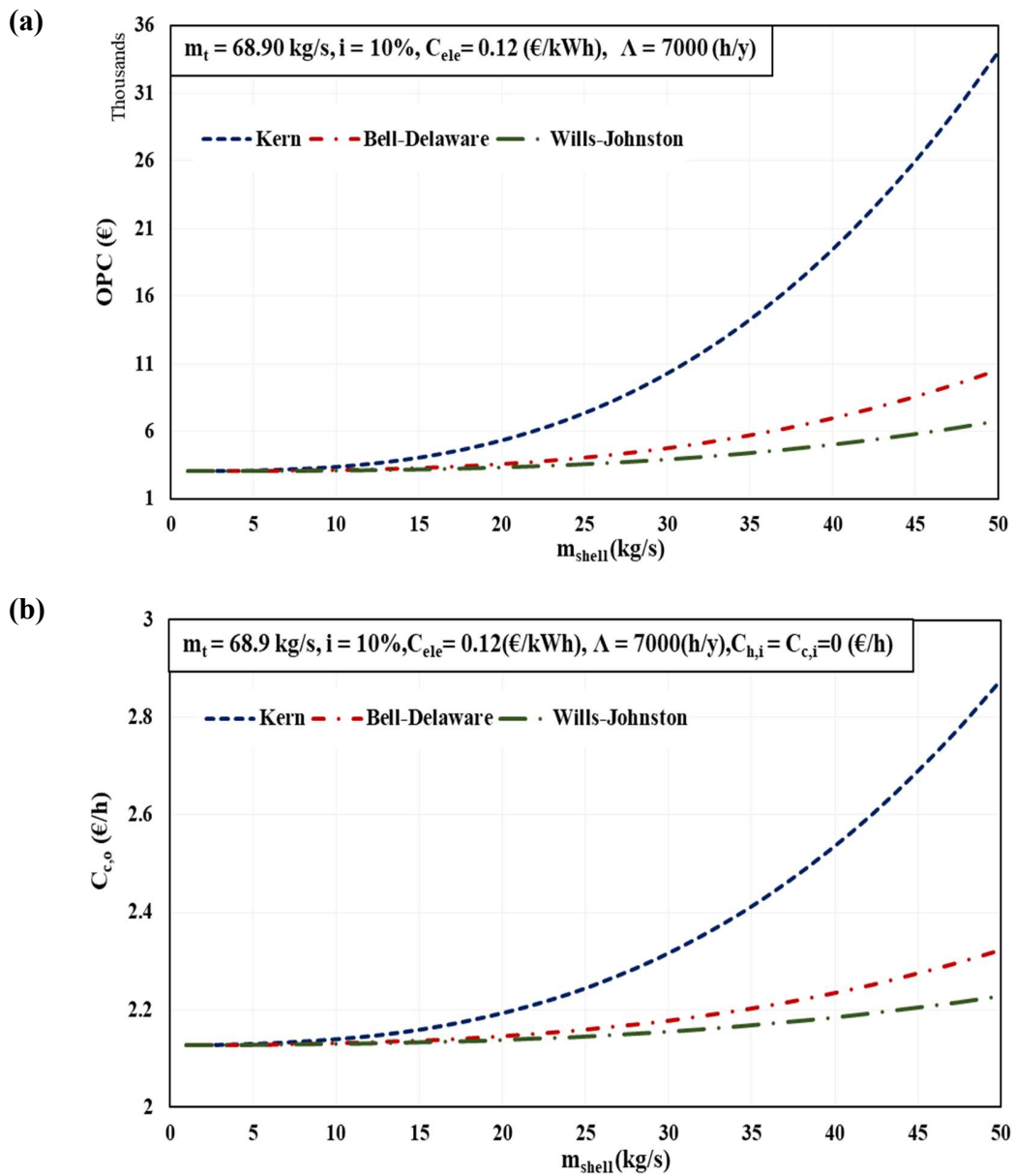


**Figure 5.** Effect of shell-side flow rate on (a) heat transfer coefficient, (b) pressure drop, and (c)  $h/\Delta P$

497  
498



499  
500

**Figure 6.** Effect of shell-side flow rate on (a) operational cost, and (b) cold water outlet stream cost.



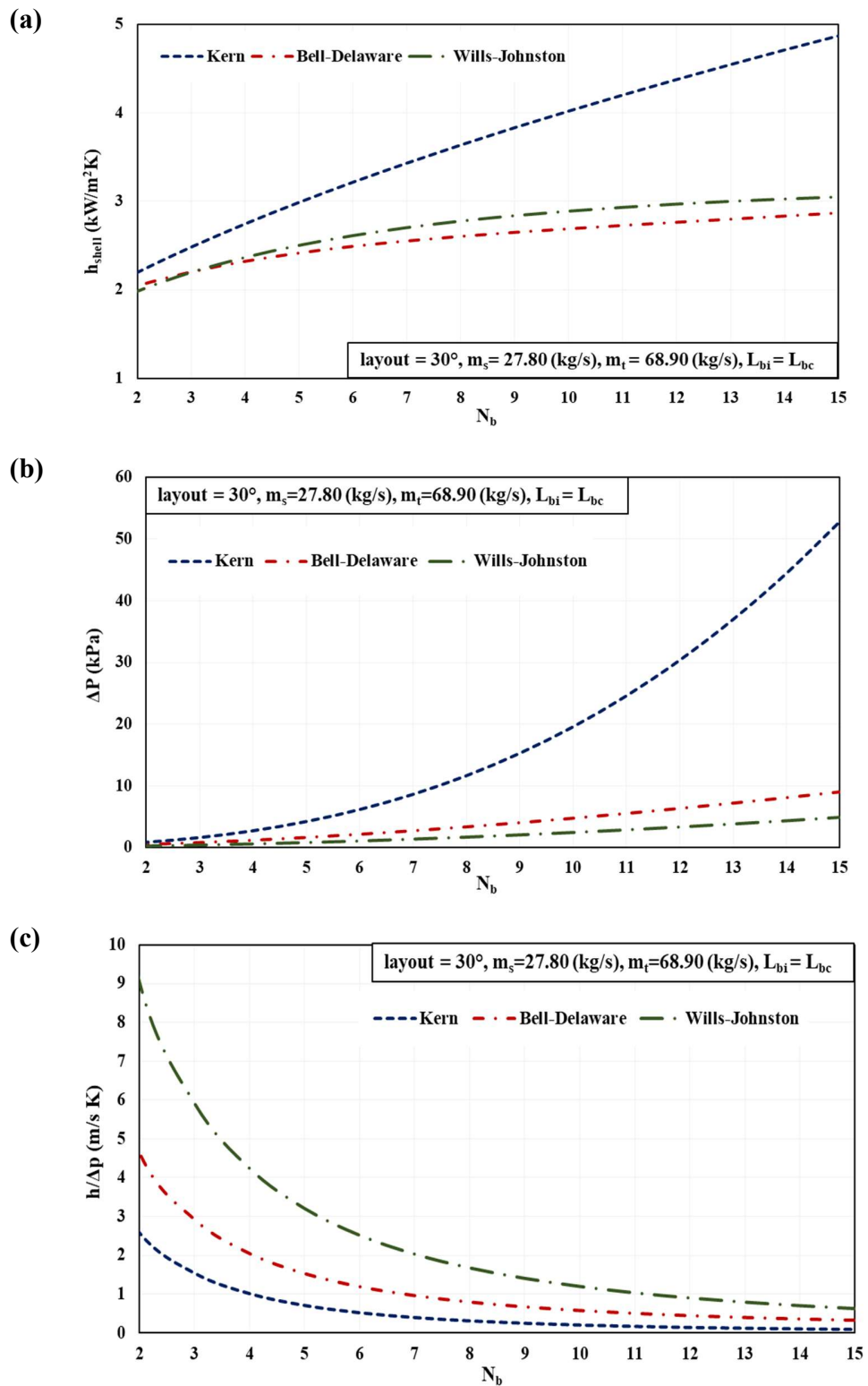
501 3.4.2. *Effect of number of baffles*

502 One of the objectives of baffles is to support the tube bundle against weight, high flow rates,  
503 and pressures to mitigate the vibrations. However, their presence also influences the shell-side  
504 thermal-hydraulic performance by obstructing the flow, as illustrated above by normalized  
505 sensitivity coefficients. Figure 7 (a) and (b) show that an increase in the number of baffles ( $N_b$ )  
506 increased the shell-side heat transfer coefficient as well as pressure drops. For example,  $h_s$   
507 increased to 3 kW/m<sup>2</sup>K for Bell-Delaware and Wills-Johnston methods and ~5 kW/m<sup>2</sup>K for the  
508 Kern method from 1.82 kW/m<sup>2</sup>K for  $N_b$  varying from 2 to 15. The corresponding variations in  
509 pressure drops are calculated as 5 kPa and 8 kPa for Bell-Delaware and Wills-Johnston and 50 kPa  
510 for the Kern method. While, the  $h/\Delta P$  factor decreased with an increase in  $N_b$ , thus showing a  
511 higher-level rise in the pressure drop than the heat transfer coefficient (refer Figure 7 (c)).

512 Besides, from a monetary viewpoint, it is noticed that (refer to Figure 8 (a)) the operational  
513 cost of STHX increased with increasing  $N_b$  due to higher pressure drop and pumping power. For  
514 instance, an increase in  $N_b$  from 2 to 15, increased the operational cost from 3,200 € to 4,900 € for  
515 Bell-Delaware and up to 4,100 € Wills-Johnston methods. While the corresponding cost for the  
516 Kern method is 14,000 €. Similarly, the cold water outlet stream cost showed a ~2.34% increase  
517 for Bell-Delaware and Wills-Johnston methods and ~12% for the Kern method. A similar trend is  
518 also observed for the other outlet stream cost with different magnitudes. It is also noticed that the  
519 diversions in thermal, hydraulic, and economic parameters calculated using Bell-Delaware and  
520 Wills-Johnston methods from the Kern method become more significant at higher  $N_b$  values. This  
521 is primarily because of the effect of not reliable pressure drop calculations of the Kern method,  
522 which amplified at a higher number of baffles.

523

524



525  
526

**Figure 7.** Effect of number of baffles on (a) shell side heat transfer coefficient (b) pressure drop, and (c)  $h/\Delta P$

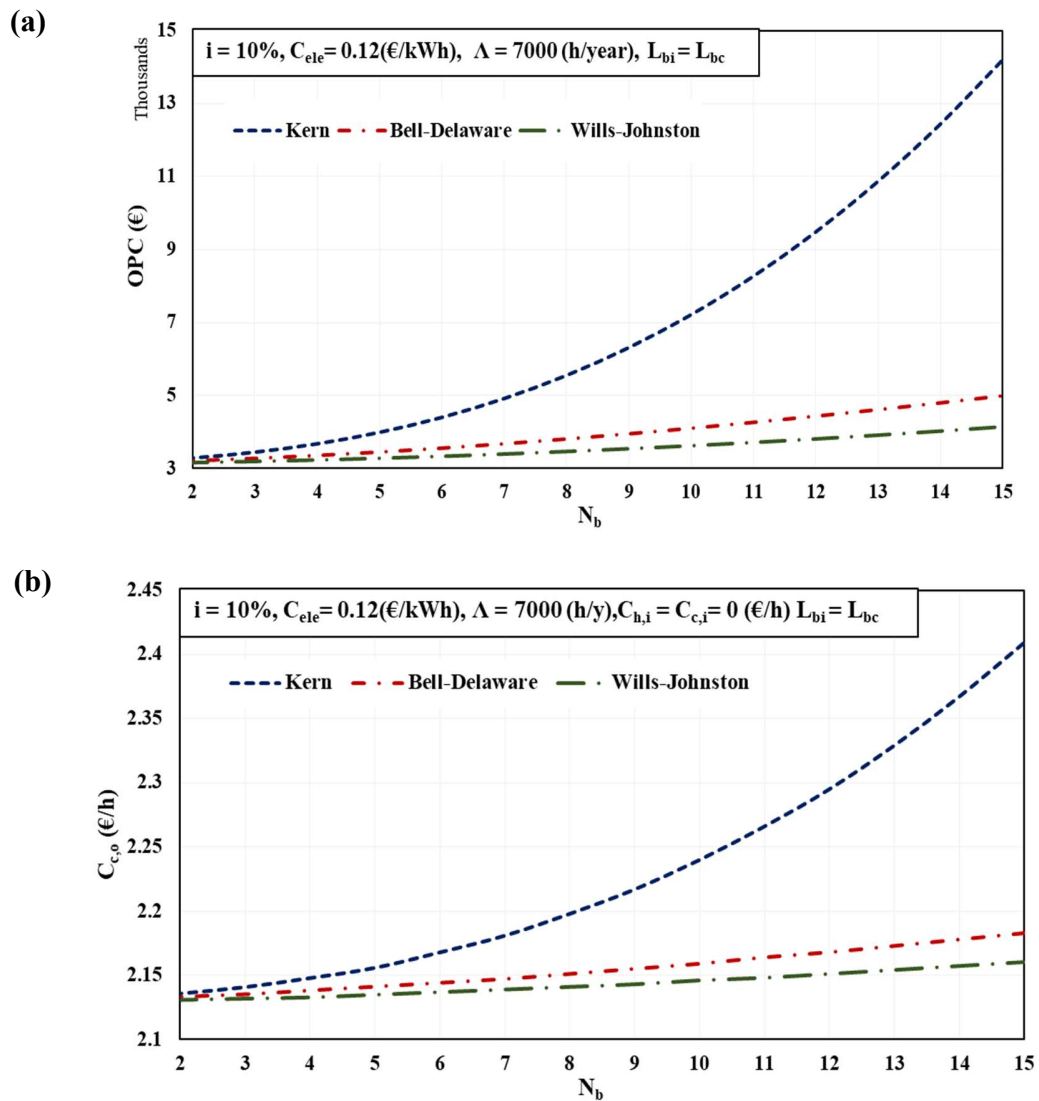


**Figure 8.** Effect of the number of baffles on (a) operational cost and (b) cold water outlet stream cost.

527  
528  
529

530 3.4.3. *Effect of fiscal parameters*

531 The conventional studies on heat exchangers are mainly focused on investigating the effects  
532 of process and design parameters on the thermodynamic and economic performance. However,  
533 analysis of the combined effect of fiscal and process parameters has gained significant attention  
534 for a rigorous thermoeconomic analysis of systems [24,26]. This is because, the systems with the  
535 same thermodynamic performance, operating in different regions and/or times with dissimilar  
536 economic policy (interest rate, energy price, chemical cost, etc.) will have substantially different  
537 operational costs [76,77]. Moreover, the sensitivity analysis also expressed a significant influence  
538 of fiscal parameters on the economic performance of STHXs in the above sections. Therefore, this  
539 investigation can satisfactorily predict an overall heat exchanger performance for the assorted  
540 operating scenarios.

541 In this regard, Figure 9 (a) and (b) illustrate the effect of the cost index factor ( $C_{\text{index}}$ ) on the  
542 total-and-stream costs. The figure shows a linear rise in the total cost ( $C_{\text{total}}$ ) and stream outlet cost  
543 over the years. For example,  $C_{\text{total}}$  of the heat exchanger configuration increased by ~70% from  
544 ~55,000 € to ~93,000 € over 30 years because of market inflation. Consequently, the stream cost  
545 surged to 2.3 €/h from 1.3 €/h during this period. A similar variation in the product cost is observed  
546 with the interest rate, as shown in Figure 9 (c). It is seen that a heat exchanger (with the same  
547 thermal-hydraulic performance) operating in two different regions with dissimilar interest rates  
548 will have significantly different product costs. For instance, the product cost of cold water outlet  
549 stream showed an increase of ~30% (from 1.6 to 2.1 €/h) for an STHX operating at interest rates  
550 of 4% and 10%, respectively.

551 Similarly, the product cost of an STHX operating at different unit electricity costs is shown in  
552 Figure 9 (d). It shows the significance of pressure drop, particularly for situations with high unit  
553 energy prices. Moreover, significant deviation in the OPC calculated using the Kern method from  
554 Bell-Delaware and Wills-Johnston method (which grow with increasing  $C_{\text{elec}}$ ) indicate rough  
555 pressure drop calculations. Besides, the chemical cost can also be an influential parameter for HXs  
556 subjected to high fouling tendency fluids. However, an accurate antifoulant cost estimation  
557 requires dynamic modeling of fouling propensity.

558

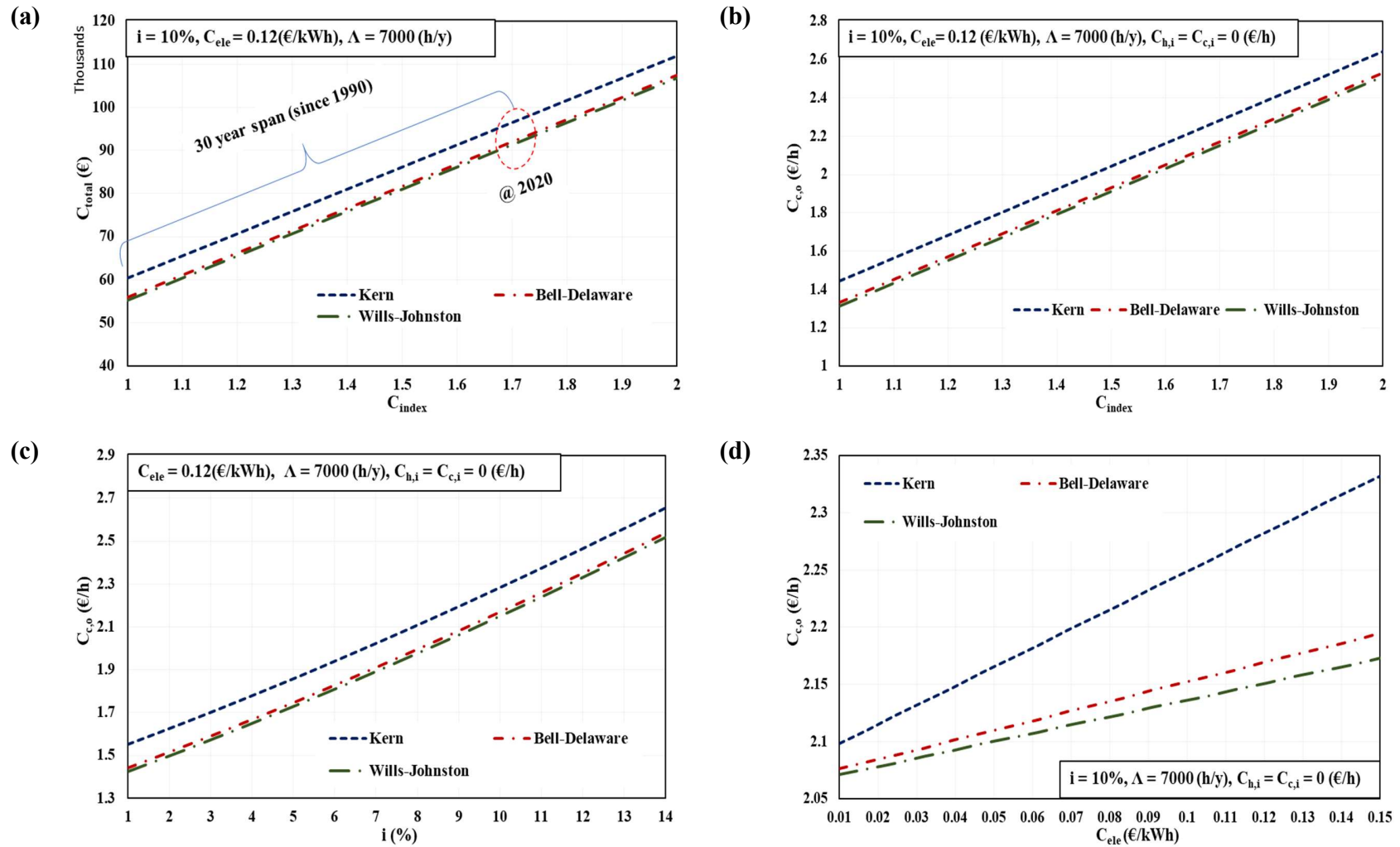
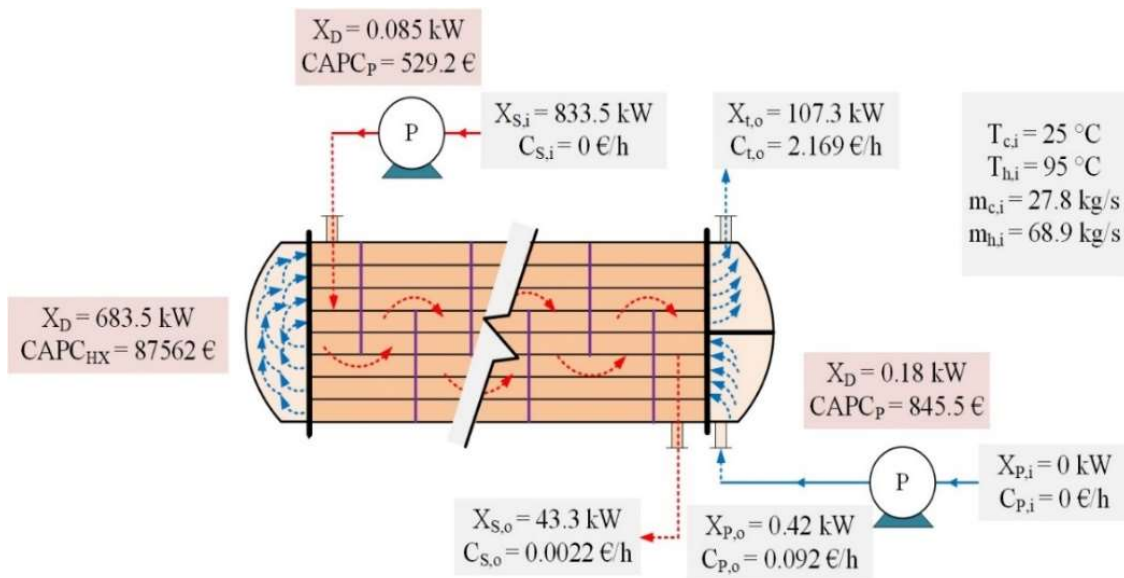


**Figure 9.** Effect of fiscal parameters (a) total cost versus cost index factor, (b) cold water outlet cost versus cost index factor, (c) cold water outlet cost versus interest rate, and (d) cold water outlet cost versus unit electricity cost.

559  
560  
561

562 3.4.4. Exergy-and-cost flow diagram

563 The exergy-and-cost flow diagram is an important pictorial illustration of thermodynamic  
 564 and monetary performance at each unique point of the system. It presents the cost (exergy and  
 565 economic) of all streams in the system at inlets and outlets of the components calculated using  
 566 fixed and recurring expenses. This diagram is particularly important for the systems with a large  
 567 number of components (e.g., power plants, desalination systems, etc.) compared to simple heat  
 568 exchangers. This is because it indicates exergy (in kW) and cost rates (in €/time), which are reliable  
 569 indicators of how efficiently the energy and economic resources are continuously utilized by each  
 570 component rather than merely relying on the investments at the system boundaries. The exergy-  
 571 and-cost flow diagram for the heat exchanger configuration considered in this study is presented  
 572 in Figure 10.



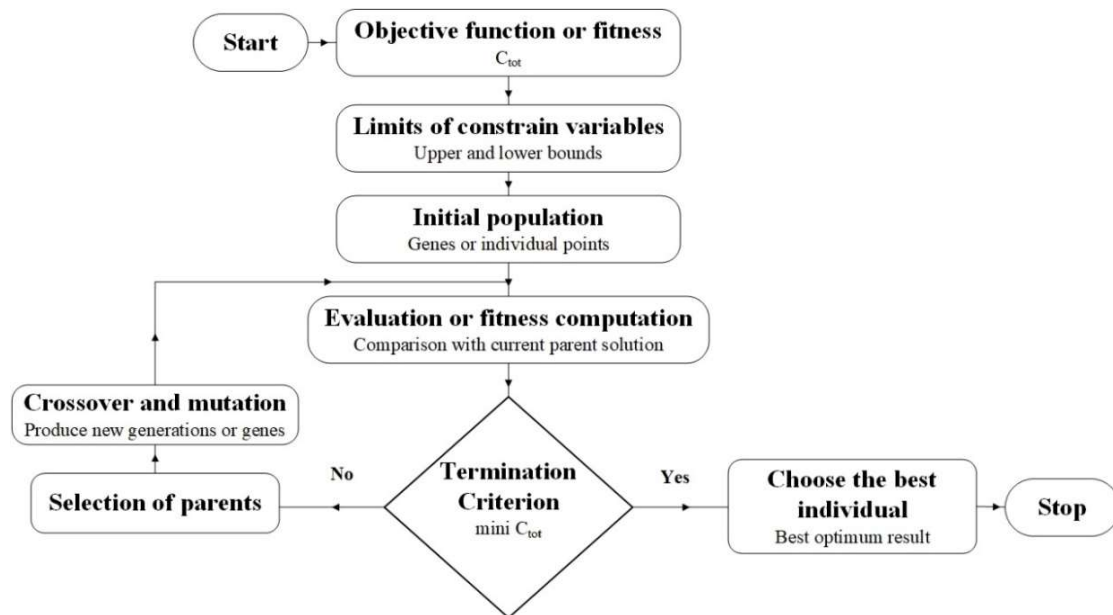
573  
 574 **Figure 10.** Exergy-and-cost flow diagram of the heat exchanger arrangement.  
 575

576 3.5. Optimization

577 After a detailed design sensitivity and parametric analyses, the optimization of STHX is  
 578 conducted using the Genetic Algorithm (GA). The GA is a biological evolution based natural  
 579 algorithm in which the survival gene (best individual point) replaces the old gene to get the  
 580 optimum solution. The objective function (fitness) is defined first, which allows each potential  
 581 solution to be evaluated. Then the estimated range of design variables and termination criteria is

582 selected, and a random initial population is developed in the range of design variables. After the  
 583 initialization of the population, the algorithm sets the arrangement of the new population (next  
 584 generation) repeatedly and perform the iterations until the termination criterion is met. Each point  
 585 (gene) contains a solution that is evaluated with the parent solution based on the fitness. If the gene  
 586 fulfills the criteria it replaces the parent solution and becomes a new parent (current best solution).  
 587 Otherwise, the algorithm selects the pervious optimum parents and produce children (next  
 588 generation or genes) by mutation or crossover of parent's and replace the population with children  
 589 to produce the next generation. The process is continued until the criteria are attained. The  
 590 termination criteria refer to either the best-optimized solution or the maximum number of  
 591 generations. The algorithm picks the best individual point with better-optimized results as a parent  
 592 and eliminates the inferior solution. This framework will guarantee that the algorithm converges  
 593 to the best individual point which will be the best-optimized solution for the selected objective  
 594 function [29,31,37]. The solution flowchart for GA is presented in Figure 11.

595 In the current study, the minimum total cost  $C_{total}$  is used as an objective function against seven  
 596 constraint variables, including tube layout, tube outside diameter, number of tubes, tube passes,  
 597 shell diameter, baffle cut, and baffle spacing. The upper and lower bounds for these constraints are  
 598 selected carefully from the literature [28,31,38,40], as summarized in Table 7. The values of  
 599 algorithm-specific parameters i.e., generations = 100, population size = 100, and mutation  
 600 probability = 0.035 are taken as reported by Sadeghzadeh et al. [37].



601  
 602 **Figure 11.** Flow chart of GA.

603 **Table 7.**

604 The lower, upper, and optimum value of the design variable for STHX [28,31,38,40].

Parameters	Constraint bounds		
	Lower	Upper	Optimum*
Layout	30°	90°	30°
Shell diameter, m	0.1	1.5	1.483
Tube outside diameter, m	0.015	0.051	0.01501
Baffle cut ratio, $B_c$	0.20	0.35	0.3141
Baffle spacing, m	0.05	0.5	0.489
Number of tube passes	1	8	1
Number of tubes	900	2000	901

605 \* calculated,

606 Note: Not all references provided all data ranges.

607 The optimization is performed for all three methods (i.e., Kern, Bell-Delaware, and Wills-  
608 Johnston), and the values for standard and optimal STHX are presented in Table 8. Owing to the  
609 highest reliability, the discussions are made concerning the Bell-Delaware method in detail. It is  
610 observed that the optimization altered the STHX performance, significantly, as indicated by  
611 various thermal, hydraulic, and economic parameters. For example, the tube side heat transfer  
612 coefficient and the shell side heat transfer coefficient decreased by ~2.2% and ~21.7%,  
613 respectively, which decreased the overall heat transfer coefficient by ~7.7%. Meanwhile, the  
614 corresponding tube- and shell-side pressure drops reduced much more significantly (than heat  
615 transfer coefficients) by ~43.8% and ~66.6%, respectively, thus decreasing the pumping power by  
616 ~50.7%.

617 Accordingly, the comprehensive thermal-hydraulic performance indicator (i.e.,  $h/\Delta P$ )  
618 increased by ~2.3 folds, indicating improved thermodynamic performance. Meanwhile, because  
619 of modifications in design parameters, the number of tubes decreased slightly, but the shell  
620 diameter increased. The optimal heat transfer area was reduced by ~26.4%, resulting in a ~20.5%  
621 cut in the capital cost. Similarly, the operational cost observed a ~50.7% reduction because of  
622 pumping power. Finally, the total cost decreased by ~22%, which reduced the cold water  
623 production (stream) cost from 2.16 to 1.68 €/h (~21%). A similar trend can also be observed for  
624 the other two methods with somewhat different magnitudes.



625 Overall, it is summarized that the sensitivity analysis and optimization of conventional  
626 STHX appreciably improved the design and analysis process. Therefore, the modern thermal  
627 system studies should be extended to normalized sensitivity analysis and optimization through any  
628 of the numerical techniques (Genetic Algorithm, Particle Swarm Optimization, etc.) rather than  
629 simply relying on conventional parametric analysis.

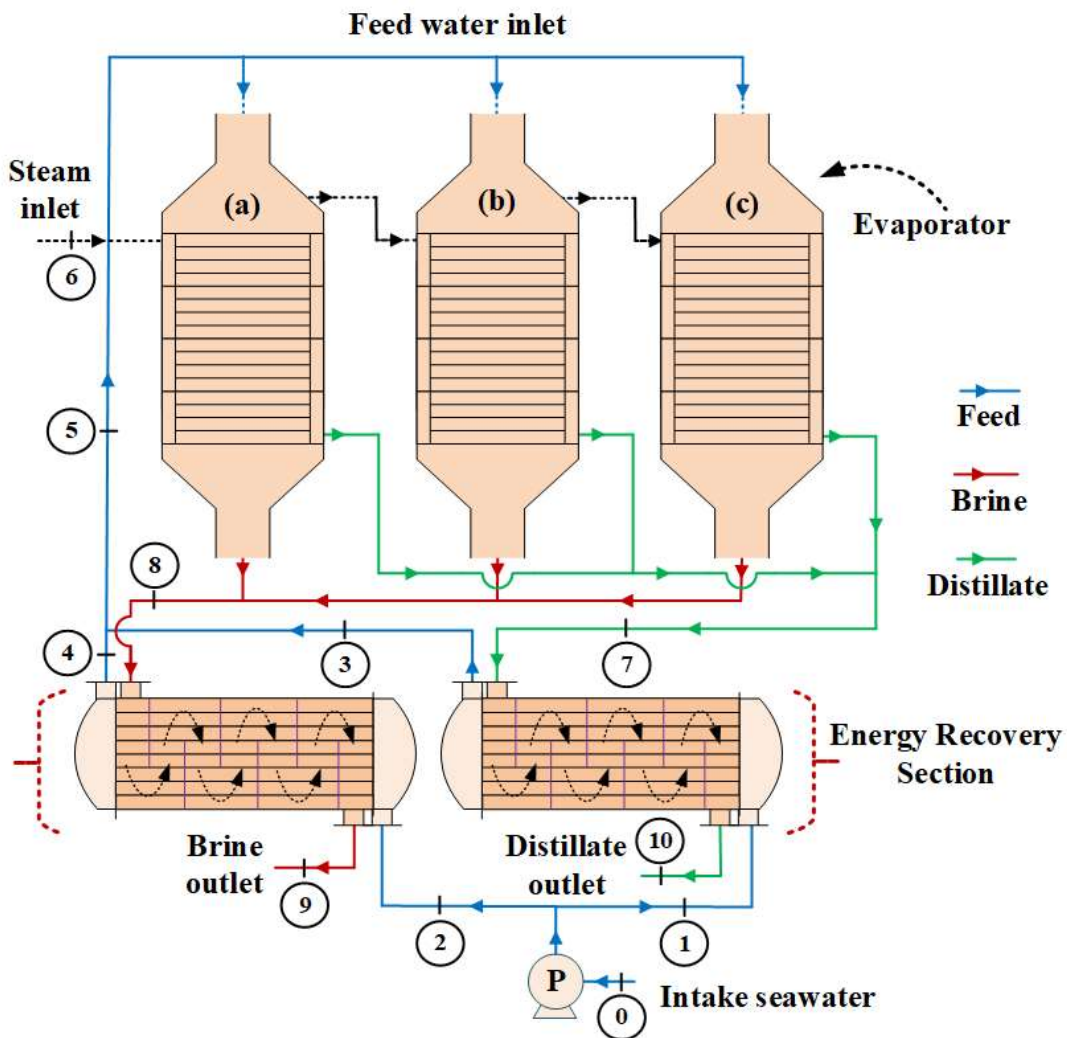
630 **Table 8.**  
631 Parameters of optimal shell-and-tube heat exchanger using a genetic algorithm.

Parameter	Kern		Bell-Delaware		Wills-Johnston	
	Standard	Optimal	Standard	Optimal	Standard	Optimal
$Re_t$	15,779	10,727	15,779	10,727	15,779	10,727
$h_t, W/m^2K$	4053	3964	4053	3964 ↓	4053	3964
$Re_s$	15,095	4974	19,651	6608	4281	2299
$h_s, W/m^2K$	4300	3110	2748	2150 ↓	2952	2623
$U, W/m^2K$	854	789	768	709 ↓	785	756.3
$\Delta P_t, Pa$	6098	3426	6098	3426 ↓	6098	3426
$\Delta P_s, Pa$	27,786	10,168	6447	2150 ↓	3257	1090
$h_s/\Delta P_s, m/s K$	0.1548	0.305	0.4262	1 ↑	0.9065	2.407
$PP, kW$	1.73	0.75	0.8648	0.426 ↓	0.7354	0.383
$X_{D total}, kW$	685	684	684	684	684	684
$A, m^2$	278.6	205	278.6	205 ↓	278.6	205
$CAPC_{HX}, €$	87,562	69,582	87,562	69,582 ↓	87,562	69,582
$CAPC_{total}, €$	89,589	70,878	88,936	70,478 ↓	88,751	70,397
$\dot{Z}_{total}, €/h$	2.083	1.648	2.068	1.639 ↓	2.064	1.637
$OPC, €$	8931	3878	4464	2200 ↓	3796	1978
$C_{total}, €$	96,492	73,460	92,025	71,782 ↓	91,357	71,560
$\dot{C}_{c,o}, €$	2.282	1.735	2.169	1.689 ↓	2.151	1.682

632 ↓: Decrease, ↑: Increase

633 4. Analysis of STHX as a preheater in a desalination system

634 Preheaters are used in thermal desalination systems to recover heat from brine and distillate  
635 streams, respectively as a brine and distillate preheaters. The recuperated energy is used to preheat  
636 the intake seawater which improves the system performance from an energy, exergy, economic,  
637 and environmental viewpoint. The schematic diagram for a conventional desalination system with  
638 STHX as an energy recovery section is shown in Figure 12. Meanwhile, it is also important to note  
639 that for more narrow temperature control and ease of maintenance, the plate and frame heat  
640 exchangers are also preferred [91]. A comprehensive theoretical framework for a component-  
641 based exergoeconomic analysis and optimization of the whole plant is presented in Eq. 47-57 [92].



642

643

**Figure 12.** Thermal desalination system with STHX as an energy recovery section.

644 The cost at the pump outlet is calculated using the capital cost of pump, electricity consumption,  
 645 and unit electricity cost as:

$$646 \quad \dot{C}_1 = \psi (\dot{C}_0 + C_{elec} \dot{W}_{Pump} + \zeta_{Pump}) \quad (47)$$

$$647 \quad \dot{C}_2 = (1 - \psi) (\dot{C}_0 + C_{elec} \dot{W}_{Pump} + \zeta_{Pump}) \quad (48)$$

648 where  $\psi$  is the feed split ratio between the two preheaters (e.g.,  $\psi = 0.5$  indicates an equal  
 649 distribution of feed in both the preheaters.

650 The feed water cost at distillate preheater and brine preheater outlet is calculated using the  
 651 capital cost of the respective preheater (i.e., STHX) and auxiliary equation as:

$$652 \quad \dot{C}_3 = \dot{C}_1 + \dot{C}_7 - \dot{C}_{10} + \zeta_{DH} \quad (49)$$

$$653 \quad \frac{\dot{C}_1}{X_1} = \frac{\dot{C}_3}{X_3} \quad (50)$$

$$654 \quad \dot{C}_4 = \dot{C}_8 + \dot{C}_2 - \dot{C}_9 + \zeta_{BH} \quad (51)$$

$$655 \quad \frac{\dot{C}_8}{X_8} = \frac{\dot{C}_9}{X_9} \quad (52)$$

656 The overall feed cost at the evaporator inlet is taken as a sum of the streams from both the  
 657 preheaters, as

$$658 \quad \dot{C}_5 = \dot{C}_3 + \dot{C}_4 \quad (53)$$

659  
 660 The distillate cost at the evaporator outlet is calculated using inlet steam cost, feed cost, and  
 661 capital cost of the evaporation section. Two auxiliary equations required to solve the evaporator  
 662 section are also given below.

$$663 \quad \dot{C}_7 = \dot{C}_5 + \dot{C}_6 - \dot{C}_8 + \zeta_{Evaporator} \quad (54)$$

$$664 \quad \frac{\dot{C}_5}{X_5} = \frac{\dot{C}_8}{X_8} \quad (55)$$

$$665 \quad \frac{\dot{C}_6}{X_6} = \frac{\dot{C}_7}{X_7} \quad (56)$$

666 Finally, the water production cost is calculated using the overall distillate cost and the water  
 667 production capacity of the plant.

668 
$$\dot{C}_{fw} (\$/\text{m}^3) = \frac{\dot{C}_9 + \dot{C}_{10} + \dot{C}_{misc}}{\dot{V}_D} \quad (57)$$

669 where,  $\dot{C}_{misc}$  is the miscellaneous cost such as blowdown, cooling, condensate, chemical, post-  
670 treatment, etc.

671 **5. Concluding remarks**

672 A liquid-phase segmental baffle shell-and-tube heat exchanger was investigated from thermal,  
673 hydraulic, exergy, and economic viewpoint. Three design approaches, i.e., Kern, Bell-Delaware,  
674 and Wills-Johnston (flow stream) were used for thermal-hydraulic modeling. An exergy-and-cost  
675 flow-based analysis procedure was presented to calculate fluid stream costs. A normalized  
676 sensitivity analysis is carried out to identify the most influential input parameters in the form of  
677 normalized sensitivity coefficients and relative contributions. Then a detailed parametric analysis  
678 was conducted to investigate the real scale effect of input parameters using the one-factor-at-a-  
679 time approach. Finally, the design was optimized for the minimum total cost by employing the  
680 Genetic Algorithm. Under the operating conditions considered in this study, some significant  
681 findings were drawn as follows.

- 682 • The flow-stream analysis method of Wills-Johnston, though used rarely, can predict shell-  
683 side thermal-hydraulic parameters reasonably close to the Bell-Delaware method ( $\pm 10\%$ ).
- 684 • Kern method is only useful for approximate preliminary sizing of STHX because of large  
685 scale over/underestimation ( $> \pm 100\%$ ) of heat transfer coefficient and pressure drops which  
686 govern the heat exchanger cost.
- 687 • The deviation of the Kern method intensified ( $\pm 200\%$ ) at a higher number of baffles and flow  
688 rates because of the augmented effects of baffles, which are not accounted for precisely in  
689 the Kern method.
- 690 • The sensitivity analysis showed that thermal performance ( $h_s$ ) of STHX is sensitive to the  
691 input parameters in the following order with normalized sensitivity coefficient (NSC)  
692 magnitudes as,  $\dot{m}_s$  (NSC: 0.372)  $>$   $T_{S,i}$  (NSC: 0.035)  $>$   $L_{bc}$  (NSC: 0.032)  $>$   $T_{S,o}$  (NSC: 0.0063)  
693 and the hydraulic performance ( $\Delta P_s$ ) as  $L_{bc}$  (NSC: 4.5)  $>$   $\dot{m}_s$  (NSC: 3.62).
- 694 • The sensitivity of operational cost of STHX for the process and fiscal parameters was  
695 observed to be in the following order  $C_{elec}$  (NSC: 0.99)  $>$   $\dot{m}_s$  (NSC: 0.78)  $>$   $L_{bc}$  (NSC: 0.41)  $>$   
696  $i$  (NSC: 0.18).
- 697 • The parametric analysis showed that an increase in the shell-side flow rate increased the heat  
698 transfer coefficient, pressure drop, and pumping power because of enhanced turbulence.

- 699 • The shell-side heat transfer coefficient per unit pressure drop decreased with increasing flow  
700 rate as well as the number of baffles that indicated a higher-order increase in the pressure  
701 drops, which in turn increased the heat exchanger operating cost.
- 702 • The heat exchanger operating cost was observed to be a strong function of fiscal parameters,  
703 i.e., cost index factor, interest rate, electricity cost, etc. Therefore, the values of these  
704 parameters should be selected carefully for reliable cost estimation.
- 705 • The exergoeconomic analysis calculated the stream exergy-and-monetary costs. It helped to  
706 develop the cost flow diagram. The final hot water production cost was calculated as 2.1 €/h.  
707 It is found to increase with increasing flow rates, the number of baffles, and the inflation rate.
- 708 • The optimization improved the STHX design appreciably by modifying the design  
709 parameters. For the optimal heat exchanger, the heat transfer area reduced by ~26.4%, capital  
710 cost by ~20.5%, operational cost by ~50.7%, total expenditure by ~22%, and the stream cost  
711 by ~21%.

## 712 **Acknowledgment**

713 The authors acknowledge the support provided by Khwaja Fareed University of Engineering  
714 and Information Technology (KFUEIT), Rahim Yar Khan. Also, Dr. Muhammad Wakil Shahzad  
715 acknowledges the support provided by Northumbria University, UK under reference #  
716 RDF20/EE/MCE/SHAHZAD. Dr. Syed Zubair would like to acknowledge the support received  
717 from King Fahd University of Petroleum & Minerals (KFUPM) through the project IN171048.  
718 Also acknowledged is the support provided by Mr. Kashif Allah Yar (an undergraduate student at  
719 the Mechanical Engineering Department KFUEIT), for organizing the literature and numerical  
720 model.

721

722 **Nomenclature**

$A$	constant
$A$	heat transfer area, m <sup>2</sup>
$B$	constant
$B_c$	baffle cut, %
$b_o$	constant used in eq. (3)
$\dot{C}$	product cost, (€/h)
$C_{total}$	total cost of equipment, €
$C_o$	annual current cost, €/y
$C_{ele}$	cost of electricity, €/kWh
$C_p$	specific heat capacity, J/kg.K
$D$	diameter, m
$D_w$	hydraulic diameter, m
$\bar{e}x$	specific exergy, k.J/kg
$F$	friction factor
$G$	mass flux, kg/s.m <sup>2</sup>
$G_w$	mass flux in the window area, kg/s.m <sup>2</sup>
$H$	heat transfer coefficient, W/m <sup>2</sup> .K
$h'$	enthalpy, kJ
$I$	interest rate, %
$J$	the correction factor for the heat transfer coefficient
$K$	thermal conductivity, W/m.K
$K_f$	parameter in Appendix A-2
$L_{bi}$	inlet baffle spacing, m
$L_{bo}$	outlet baffle spacing, m
$L_{bc}$	central baffle spacing, m
$L_t$	tube length, m
$\dot{m}$	flow rate, kg/s
$N$	flow coefficient, kg <sup>-1</sup> .m <sup>-1</sup>
$n_y$	equipment life, year
$N_b$	number of baffles
$N_c$	total number of tube rows in cross-flow
$Nu$	Nusselt number

$N_t$	total number of tubes
$N_p$	number of tube passes
$p_c$	constant in Eq. (4)
$P$	parameter in Eq. (31)
$PP$	pumping power, W
$Pr$	Prandtl number,
$P_t$	tube pitch, m
$\Delta P$	pressure drop, Pa
$R$	correction factor for pressure drop
$S$	entropy, J/K
$S$	leakage areas, m <sup>2</sup>
$\dot{S}_{gen}$	entropy generation rate, W/K
$Tb$	baffle thickness, m
$Re$	Reynolds number
$R_f$	fouling resistance, m <sup>2</sup> .K/W
$T_{in}$	temperature inlet, °C
$T_{out}$	temperature outlet, °C
$U$	overall heat transfer coefficient, W/m <sup>2</sup> .K
$V$	velocity, m/s
$W$	weight, kg
$\dot{W}_p$	pump work, kW
$X$	exergy, kW
$X_D$	exergy destruction, kW
$\dot{Z}$	annual rate of capital investment, €/y

### Greek Symbols

$\zeta$	rate of fixed cost, €/s
$B$	layout, deg
$\varepsilon$	effectiveness
$\theta_{cut}$	angle between centerline and baffle cut, deg
$\rho$	density, kg/m <sup>3</sup>
$\Phi$	viscosity correction factor
$\mu$	viscosity, Pa.s



$\psi$  is the feed split ration

$A$  operation hours, hour

$H$  efficiency

### Subscripts

$0$  dead state

$A$  combined coefficient

$bl$  ideal tube bundle

$B$  bypass

$C$  cross-flow or central baffle spacing

$ctl$  center-line tube

$c,i$  cold in

$c,o$  cold out

$Cb$  combined coefficient

$Cr$  cross-flow

$E$  equivalent or exist baffle

$h,i$  hot in

$h,o$  hot out

$I$  in

$L$  leakage

$M$  cross-flow area at the centerline

$O$  out

$P$  combined coefficient

$R$  laminar flow

$S$  shell

$Sb$  shell-to-baffle

$S$  unequal baffle spacing

$T$  tube

$Tb$  tube-to-baffle

$t,i$  tube inside

$t,o$  tube outside

$W$  wall or window

### Abbreviations

$BH$  brine heater

$CAPC$  capital cost

<i>CEPCI</i>	chemical engineering plant cost index
<i>CRF</i>	capital recovery factor
<i>DH</i>	distillate heater
<i>HXs</i>	heat exchangers
<i>OFAT</i>	one-factor-at-a-time
<i>OPC</i>	operational cost
<i>STHX</i>	shell and tube heat exchanger

723

724

725

726 **References**

- 727 [1] Catrini P, Cipollina A, Micale G, Piacentino A, Tamburini A. Exergy analysis and  
728 thermoeconomic cost accounting of a Combined Heat and Power steam cycle integrated  
729 with a Multi Effect Distillation- Thermal Vapour Compression desalination plant. *Energy*  
730 *Convers Manag* 2017;149:950–65.
- 731 [2] Chitgar N, Emadi MA, Chitsaz A, Rosen MA. Investigation of a novel multigeneration  
732 system driven by a SOFC for electricity and fresh water production. *Energy Convers Manag*  
733 2019;196:296–310.
- 734 [3] Gholizadeh T, Vajdi M, Rostamzadeh H. Exergoeconomic optimization of a new  
735 trigeneration system driven by biogas for power, cooling, and freshwater production.  
736 *Energy Convers Manag* 2020;205:112417.
- 737 [4] Serth RW, Lestina T. *Process Heat Transfer (Second Edition) Principles, Applications and*  
738 *Rules of Thumb*. 2014.
- 739 [5] Costa ALH, Queiroz EM. Design optimization of shell-and-tube heat exchangers. *Appl*  
740 *Therm Eng* 2008;28:1798–805. doi:10.1016/j.applthermaleng.2007.11.009.
- 741 [6] Gulenoglu C, Akturk F, Aradag S, Uzol NS, Kakac S. Experimental comparison of  
742 performances of three different plates for gasketed plate heat exchangers. *Int J Therm Sci*  
743 2014;75:249–56. doi:10.1016/j.ijthermalsci.2013.06.012.
- 744 [7] Rao RV, Patel V. Multi-objective optimization of heat exchangers using a modified  
745 teaching-learning-based optimization algorithm. *Appl Math Model* 2013;37:1147–62.  
746 doi:10.1016/j.apm.2012.03.043.
- 747 [8] Zhang Z, Ma D, Fang X, Gao X. Experimental and numerical heat transfer in a helically  
748 baffled heat exchanger combined with one three-dimensional finned tube. *Chem Eng*  
749 *Process Process Intensif* 2008;47:1738–43.
- 750 [9] Thome JR. *Engineering Data Book III*. Wolverine Tune, Inc.; 2004.
- 751 [10] El Maakoul A, Laknizi A, Saadeddine S, El Metoui M, Zaitte A, Meziane M, et al. Numerical  
752 comparison of shell-side performance for shell and tube heat exchangers with trefoil-hole,  
753 helical and segmental baffles. *Appl Therm Eng* 2016;109:175–85.  
754 doi:10.1016/j.applthermaleng.2016.08.067.
- 755 [11] Ambekar AS, Sivakumar R, Anantharaman N, Vivekenandan M. CFD simulation study of  
756 shell and tube heat exchangers with different baffle segment configurations. *Appl Therm*  
757 *Eng* 2016;108:999–1007. doi:10.1016/j.applthermaleng.2016.08.013.
- 758 [12] Falav Jozaei A, Baheri A, Hafshejani MK, Arad A. Optimization of baffle spacing on heat  
759 transfer, pressure drop and estimated price in a shell-and-tube heat exchanger. *World Appl*  
760 *Sci J* 2012;18:1727–36. doi:10.5829/idosi.wasj.2012.18.12.2484.
- 761 [13] Abdelkader BA, Zubair SM. The effect of a number of baffles on the performance of shell-  
762 and-tube heat exchangers. *Heat Transf Eng* 2019;40:39–52.  
763 doi:10.1080/01457632.2017.1404806.

- 764 [14] Gao B, Bi Q, Nie Z, Wu J. Experimental study of effects of baffle helix angle on shell-side  
765 performance of shell-and-tube heat exchangers with discontinuous helical baffles. *Exp*  
766 *Therm Fluid Sci* 2015;6:48–57, Nov.
- 767 [15] Abdelkader BA, Jamil MA, Zubair SM. Thermal-Hydraulic Characteristics of Helical  
768 Baffle Shell-and-Tube Heat Exchangers. *Heat Transf Eng* 2019.  
769 doi:10.1080/01457632.2019.1611135.
- 770 [16] Kayabasi E, Kurt H. Simulation of heat exchangers and heat exchanger networks with an  
771 economic aspect. *Eng Sci Technol an Int J* 2018;21:70–6. doi:10.1016/j.jestch.2018.02.006.
- 772 [17] Roy U, Majumder M. Economic optimization and energy analysis in shell and tube heat  
773 exchanger by meta-heuristic approach. *Vacuum* 2019;166:413–8.  
774 doi:10.1016/j.vacuum.2018.12.052.
- 775 [18] Selbaş R, Kizilkan Ö, Reppich M. A new design approach for shell-and-tube heat  
776 exchangers using genetic algorithms from economic point of view. *Chem Eng Process*  
777 *Process Intensif* 2006;45:268–75. doi:10.1016/j.cep.2005.07.004.
- 778 [19] Vasconcelos Segundo EH de, Mariani VC, Coelho L dos S. Design of heat exchangers using  
779 Falcon Optimization Algorithm. *Appl Therm Eng* 2019;156:119–44.  
780 doi:10.1016/j.applthermaleng.2019.04.038.
- 781 [20] Bejan A, Tsatsaronis G, Moran M. *Thermal Design and Optimization*. Wiley; 1996.
- 782 [21] Lazzaretto A, Tsatsaronis G. SPECO: A systematic and general methodology for calculating  
783 efficiencies and costs in thermal systems. *Energy* 2006;31:1257–89.
- 784 [22] Keshavarzian S, Rocco M V., Gardumi F, Colombo E. Practical approaches for applying  
785 thermoeconomic analysis to energy conversion systems: Benchmarking and comparative  
786 application. *Energy Convers Manag* 2017;150:532–44.
- 787 [23] Hajabdollahi H, Ahmadi P, Dincer I. Thermo-economic optimization of a shell and tube  
788 condenser using both genetic algorithm and particle swarm. *Int J Refrig* 2011;34:1066–76.  
789 doi:10.1016/j.ijrefrig.2011.02.014.
- 790 [24] Jamil MA, Zubair SM. Design and analysis of a forward feed multi-effect mechanical vapor  
791 compression desalination system : An exergo-economic approach. *Energy* 2017;140:1107–  
792 20. doi:10.1016/j.energy.2017.08.053.
- 793 [25] Zhang C, Liu C, Wang S, Xu X, Li Q. Thermo-economic comparison of subcritical organic  
794 Rankine cycle based on different heat exchanger configurations. *Energy* 2017;123:728–41.  
795 doi:10.1016/j.energy.2017.01.132.
- 796 [26] Jamil MA, Elmutasim SM, Zubair SM. Exergo-economic analysis of a hybrid  
797 humidification dehumidification reverse osmosis (HDH-RO) system operating under  
798 different retrofits. *Energy Convers Manag* 2018;158:286–97.
- 799 [27] Ghazi M, Ahmadi P, Sotoodeh AF, Taherkhani A. Modeling and thermo-economic  
800 optimization of heat recovery heat exchangers using a multimodal genetic algorithm.  
801 *Energy Convers Manag* 2012;58:149–56. doi:10.1016/j.enconman.2012.01.008.

- 802 [28] Caputo AC, Pelagagge PM, Salini P. Heat exchanger design based on economic  
803 optimisation. *Appl Therm Eng* 2008;28:1151–9.
- 804 [29] Guo J, Cheng L, Xu M. Optimization design of shell-and-tube heat exchanger by entropy  
805 generation minimization and genetic algorithm. *Appl Therm Eng* 2009;29:2954–60.  
806 doi:10.1016/j.applthermaleng.2009.03.011.
- 807 [30] Guo J, Xu M, Cheng L. The application of field synergy number in shell-and-tube heat  
808 exchanger optimization design. *Appl Energy* 2009;86:2079–87.  
809 doi:10.1016/j.apenergy.2009.01.013.
- 810 [31] Ponce-Ortega JM, Serna-González M, Jiménez-Gutiérrez A. Use of genetic algorithms for  
811 the optimal design of shell-and-tube heat exchangers. *Appl Therm Eng* 2009;29:203–9.  
812 doi:10.1016/j.applthermaleng.2007.06.040.
- 813 [32] Patel VK, Rao R V. Design optimization of shell-and-tube heat exchanger using particle  
814 swarm optimization technique. *Appl Therm Eng* 2010;30:1417–25.  
815 doi:10.1016/j.applthermaleng.2010.03.001.
- 816 [33] Şencan Şahin A, Kiliç B, Kiliç U. Design and economic optimization of shell and tube heat  
817 exchangers using Artificial Bee Colony (ABC) algorithm. *Energy Convers Manag*  
818 2011;52:3356–62. doi:10.1016/j.enconman.2011.07.003.
- 819 [34] Hadidi A, Hadidi M, Nazari A. A new design approach for shell-and-tube heat exchangers  
820 using imperialist competitive algorithm (ICA) from economic point of view. *Energy*  
821 *Convers Manag* 2013;67:66–74. doi:10.1016/j.enconman.2012.11.017.
- 822 [35] Hadidi A, Nazari A. Design and economic optimization of shell-and-tube heat exchangers  
823 using biogeography-based (BBO) algorithm. *Appl Therm Eng* 2013;51:1263–72.  
824 doi:10.1016/j.applthermaleng.2012.12.002.
- 825 [36] Asadi M, Song Y, Sunden B, Xie G. Economic optimization design of shell-and-tube heat  
826 exchangers by a cuckoo-search-algorithm. *Appl Therm Eng* 2014;73:1032–40.  
827 doi:10.1016/j.applthermaleng.2014.08.061.
- 828 [37] Sadeghzadeh H, Ehyaei MA, Rosen MA. Techno-economic optimization of a shell and tube  
829 heat exchanger by genetic and particle swarm algorithms. *Energy Convers Manag*  
830 2015;93:84–91. doi:10.1016/j.enconman.2015.01.007.
- 831 [38] Khosravi R, Khosravi A, Nahavandi S, Hajabdollahi H. Effectiveness of evolutionary  
832 algorithms for optimization of heat exchangers. *Energy Convers Manag* 2015;89:281–8.  
833 doi:10.1016/j.enconman.2014.09.039.
- 834 [39] Mohanty DK. Application of firefly algorithm for design optimization of a shell and tube  
835 heat exchanger from economic point of view. *Int J Therm Sci* 2016;102:228–38.  
836 doi:10.1016/j.ijthermalsci.2015.12.002.
- 837 [40] Hajabdollahi H, Naderi M, Adimi S. A comparative study on the shell and tube and gasket-  
838 plate heat exchangers: The economic viewpoint. *Appl Therm Eng* 2016;92:271–82.
- 839 [41] Dhavle S V., Kulkarni AJ, Shastri A, Kale IR. Design and economic optimization of shell-  
840 and-tube heat exchanger using cohort intelligence algorithm. *Neural Comput Appl*

- 841 2018;30:111–25. doi:10.1007/s00521-016-2683-z.
- 842 [42] Wen J, Yang H, Jian G, Tong X, Li K, Wang S. Energy and cost optimization of shell and  
843 tube heat exchanger with helical baffles using Kriging metamodel based on MOGA. *Int J*  
844 *Heat Mass Transf* 2016;98:29–39, Jul.
- 845 [43] Rao RV, Saroj A. Constrained economic optimization of shell-and-tube heat exchangers  
846 using elitist-Jaya algorithm. *Energy* 2017;128:785–800. doi:10.1016/j.energy.2017.04.059.
- 847 [44] Vasconcelos Segundo EH de, Amoroso AL, Mariani VC, Coelho L dos S. Economic  
848 optimization design for shell-and-tube heat exchangers by a Tsallis differential evolution.  
849 *Appl Therm Eng* 2017;111:143–51. doi:10.1016/j.applthermaleng.2016.09.032.
- 850 [45] Tharakeshwar TK, Seetharamu KN, Durga Prasad B. Multi-objective optimization using  
851 bat algorithm for shell and tube heat exchangers. *Appl Therm Eng* 2017;110:1029–38.  
852 doi:10.1016/j.applthermaleng.2016.09.031.
- 853 [46] Mirzaei M, Hajabdollahi H, Fadakar H. Multi-objective optimization of shell-and-tube heat  
854 exchanger by constructal theory. *Appl Therm Eng* 2017;125:9–19.  
855 doi:10.1016/j.applthermaleng.2017.06.137.
- 856 [47] Iyer VH, Mahesh S, Malpani R, Sapre M, Kulkarni AJ. Adaptive Range Genetic Algorithm:  
857 A hybrid optimization approach and its application in the design and economic optimization  
858 of Shell-and-Tube Heat Exchanger. *Eng Appl Artif Intell* 2019;85:444–61.  
859 doi:10.1016/j.engappai.2019.07.001.
- 860 [48] Sai JP, Rao BN. Efficiency and economic optimization of shell and tube heat exchanger  
861 using bacteria foraging algorithm. *SN Appl Sci* 2020;2:1–7. doi:10.1007/s42452-019-1798-  
862 0.
- 863 [49] Sinnott R, Towler G. *Chemical Engineering Design*. 2nd ed. 1993.
- 864 [50] Fraas AP. *Heat Exchanger Design*. New York: John Wiley & Sons; 1989.
- 865 [51] Peters MS, Timmerhaus KD. *Plant Design and Economics for Chemical Engineers*. 4th ed.  
866 McGraw-Hill; 1991.
- 867 [52] Kern DQ. *Process Heat Transfer*. McGraw-Hill; 1950.
- 868 [53] Palen JW, Taborek J. Solution of shell side flow pressure drop and heat transfer by stream  
869 analysis method, *Chem. Eng. Prog. Symp. Ser.*, vol. 65, no. 93, pp. 53-63. 1969.
- 870 [54] Tsatsaronis G. Definitions and nomenclature in exergy analysis and exergoeconomics.  
871 *Energy* 2007;32:249–53.
- 872 [55] Fitzsimons L, Corcoran B, Young P, Foley G. Exergy analysis of water purification and  
873 desalination: A study of exergy model approaches. *Desalination* 2015;359:212–24.
- 874 [56] Sharqawy MH, Lienhard V JH, Zubair SM. Thermophysical properties of seawater: a  
875 review of existing correlations and data. *Desalin Water Treat* 2010;16:354–80.
- 876 [57] Sharqawy MH, Lienhard V JH, Zubair SM. On exergy calculations of seawater with  
877 applications in desalination systems. *Int J Therm Sci* 2011;50:187–96.

- 878 [58] Nayar KG, Sharqawy MH, Banchik LD, Lienhard V JH. Thermophysical properties of  
879 seawater: A review and new correlations that include pressure dependence. *Desalination*  
880 2016;390:1–24.
- 881 [59] El-Sayed YM. *The Thermoconomics of Energy Conversions*. Amsterdam: Elsevier; 2003.
- 882 [60] El-Sayed YM. Designing desalination systems for higher productivity. *Desalination*  
883 2001;134:129–58.
- 884 [61] Shabani MR, Yekta RB. Chemical processes equipment cost estimation using parametric  
885 models. *Cost Eng* 2006;48:26–32.
- 886 [62] Turton R, Bailie RC, Whiting WB, Shaeiwitz JA, Bhattacharyya D. *Analysis, Synthesis,*  
887 *and Design of Chemical Processes*. 4th ed. Old Tappan, NJ, USA: Prentis Hall; 2013.
- 888 [63] Li YR, Du MT, Wu CM, Wu SY, Liu C, Xu JL. Economical evaluation and optimization  
889 of subcritical organic Rankine cycle based on temperature matching analysis. *Energy*  
890 2014;68:238–47.
- 891 [64] Fettaka S, Thibault J, Gupta Y. Design of shell-and-tube heat exchangers using  
892 multiobjective optimization. *Int J Heat Mass Transf* 2013;60:343–54.
- 893 [65] Li J, Yang Z, Hu S, Yang F, Duan Y. Effects of shell-and-tube heat exchanger arranged  
894 forms on the thermo-economic performance of organic Rankine cycle systems using  
895 hydrocarbons. *Energy Convers Manag* 2020;203:112248.  
896 doi:10.1016/j.enconman.2019.112248.
- 897 [66] Hall SG, Ahmad S, Smith R. Capital cost targets for heat exchanger networks comprising  
898 mixed materials of construction, pressure ratings and exchanger types. *Comput Chem Eng*  
899 1990;14:319–35.
- 900 [67] Taal M, Bulatov I, Kleme J, Stehl P. Cost estimation and energy price forecasts for  
901 economic evaluation of retrofit projects. *Appl Therm Eng* 2003;23:1819–35.
- 902 [68] Sanaye S, Hajabdollahi H. Multi-objective optimization of shell and tube heat exchangers.  
903 *Appl Therm Eng* 2010;30:1937–45. doi:10.1016/j.applthermaleng.2010.04.018.
- 904 [69] Azad AV, Amidpour M. Economic optimization of shell and tube heat exchanger based on  
905 constructal theory. *Energy* 2011;36:1087–96. doi:10.1016/j.energy.2010.11.041.
- 906 [70] Loh HP, Lyons J, White CW. *Process Equipment Cost Estimation, Final Report*. 2002.
- 907 [71] Tremblay PW-, Gosselin L. Minimizing shell-and-tube heat exchanger cost with genetic  
908 algorithms and considering maintenance. *Int J Energy Res* 2007;31:867–85.
- 909 [72] Rao RV, Saroj A. Economic optimization of shell-and-tube heat exchanger using Jaya  
910 algorithm with maintenance consideration. *Appl Therm Eng* 2017;116:473–87.  
911 doi:10.1016/j.applthermaleng.2017.01.071.
- 912 [73] Caputo AC, Pelagagge PM, Salini P. Manufacturing cost model for heat exchangers  
913 optimization. *Appl Therm Eng* 2016;94:513–33.  
914 doi:10.1016/j.applthermaleng.2015.10.123.

- 915 [74] Vataavuk WM. Updating the Cost Index. *Chem Eng* 2002;62–70.
- 916 [75] Jenkins S. 2019 Chemical engineering plant cost index annual average 2020.  
917 <https://www.chemengonline.com/2019-chemical-engineering-plant-cost-index-annual->  
918 [average/](https://www.chemengonline.com/2019-chemical-engineering-plant-cost-index-annual-) (accessed April 9, 2020).
- 919 [76] Jamil MA, Zubair SM. On thermoeconomic analysis of a single-effect mechanical vapor  
920 compression desalination system. *Desalination* 2017;420:292–307.
- 921 [77] Jamil MA, Zubair SM. Effect of feed flow arrangement and number of evaporators on the  
922 performance of multi-effect mechanical vapor compression desalination systems.  
923 *Desalination* 2018;429:76–87.
- 924 [78] Nafey AS, Fath HES, Mabrouk AA. Exergy and thermoeconomic evaluation of MSF  
925 process using a new visual package. *Desalination* 2006;201:224–40.
- 926 [79] Mabrouk AA, Nafey AS, Fath HES. Thermoeconomic analysis of some existing  
927 desalination processes. *Desalination* 2007;205:354–73.
- 928 [80] El-Emam RS, Dincer I. Thermodynamic and thermoeconomic analyses of seawater reverse  
929 osmosis desalination plant with energy recovery. *Energy* 2014;64:154–63.
- 930 [81] Rosen M a. A concise review of exergy-based economic methods. *Int. Conf. Energy*  
931 *Environ.*, 2008, p. 9.
- 932 [82] Qureshi BA, Zubair SM. A comprehensive design and rating study of evaporative coolers  
933 and condensers. Part II. Sensitivity analysis. *Int J Refrig* 2006;29:659–68.
- 934 [83] Kitchell JF, Stewart DJ, Weininger D. Applications of a Bioenergetics Model to Yellow  
935 Perch ( *Perca flavescens* ) and Walleye ( *Stizostedion vitreum vitreum* ). *J Fish Res Board*  
936 *Canada* 1977;34:1922–35.
- 937 [84] Hussaini IS, Zubair SM, Antar MA. Area allocation in multi-zone feedwater heaters. *Energy*  
938 *Convers Manag* 2007;48:568–75. doi:10.1016/j.enconman.2006.06.003.
- 939 [85] Kim JH, Simon TW. Journal of heat transfer policy on reporting uncertainties in  
940 experimental measurements and results. *J Heat Transfer* 1993;115:5–6.  
941 doi:10.1115/1.2910670.
- 942 [86] Taylor BN, Kuyatt CE. Guidelines for evaluating and expressing the uncertainty of NIST  
943 measurement results, Gaithersburg, MD, U.S. Departmente of Commerce, Technology  
944 Administration, National Institute of Standards and Technology. 1994.
- 945 [87] Masi M, Fogliani S, Carrà S. Sensitivity analysis on indium phosphide liquid encapsulated  
946 Czochralski growth. *Cryst Res Technol* 1999;34:1157–67.
- 947 [88] James CA, Taylor RP, Hodge BK. The application of uncertainty analysis to cross-flow heat  
948 exchanger performance predictions. *Heat Transf Eng* 1995;16:50–62.
- 949 [89] James CA, Taylor RP, Hodge BK. Analysis and design of energy systems. 3rd ed. Prentice  
950 Hall, Englewood Cliffs, NJ; 1998.
- 951 [90] Serth RW. Process Heat Transfer- Principles and Application. 1st ed. Amsterdam: Elsevier



952 Science and Technology Books; 2007.

953 [91] Jamil MA, Din ZU, Goraya TS, Yaqoob H, Zubair SM. Thermal-hydraulic characteristics  
954 of gasketed plate heat exchangers as a preheater for thermal desalination systems. Energy  
955 Convers Manag 2020;205:112425.

956 [92] Jamil MA, Shahzad MW, Zubair SM. A comprehensive framework for thermoeconomic  
957 analysis of desalination systems. Energy Convers Manag 2020;222:113188.

958

959

960 **Appendix: Tables for correction factors, constants, and coefficients for Bell-Delaware and**  
 961 **Wills-Johnston methods**

962 **Table A.1.**

963 Empirical coefficients for  $j_i$  and  $f_i$  [9]

<b>Layout</b>	<b>Re</b>	<b>a<sub>1</sub></b>	<b>a<sub>2</sub></b>	<b>a<sub>3</sub></b>	<b>a<sub>4</sub></b>	<b>b<sub>1</sub></b>	<b>b<sub>2</sub></b>	<b>b<sub>3</sub></b>	<b>b<sub>4</sub></b>
<b>30°</b>	$10^5-10^4$	0.321	-0.388	1.450	0.519	0.372	-0.123	7.00	0.500
	$10^4-10^3$	0.321	-0.388			0.486	-0.152		
	$10^3-10^2$	0.593	-0.477			4.570	-0.476		
	$10^2-10$	1.360	-0.657			45.10	-0.973		
	<10	1.400	-0.667			48.00	-1.00		
<b>45°</b>	$10^5-10^4$	0.370	-0.396	1.930	0.500	0.303	-0.126	6.59	0.520
	$10^4-10^3$	0.370	-0.396			0.333	-0.136		
	$10^3-10^2$	0.730	-0.500			3.500	-0.476		
	$10^2-10$	0.498	-0.656			26.20	-0.913		
	<10	1.550	-0.667			32.00	-1.00		
<b>90°</b>	$10^5-10^4$	0.370	-0.395	1.187	0.370	0.391	-0.148	6.30	0.378
	$10^4-10^3$	0.107	-0.266			0.0815	+0.022		
	$10^3-10^2$	0.408	-0.460			6.090	-0.602		
	$10^2-10$	0.900	-0.631			32.10	-0.963		
	<10	0.970	-0.667			35.00	-1.00		

964

965 **Table A.2.**

966 Bell Delaware methods correction factors for calculation of shell side heat transfer coefficient [9].

Correction factor	Accounts for	Governing equation
Baffle window flow CF ( $J_c$ )	Non-ideal cross-flow through the window zone	$J_c = 0.55 + 0.72 (1 - 2F_w)$ $F_w = (\theta_{ctl}/360) - (\sin \theta_{ctl}/2\pi), \theta_{ctl} = 2 \cos^{-1} \left( (D_s/D_{ctl})(1 - 2(B_c/100)) \right)$
Baffle leakage CF ( $J_L$ )	Flow-through the gaps between the baffle and shell, and the baffle and tube diameter	$J_L = 0.44 \left( 1 - \frac{S_{sb}}{S_{sb} + S_{tb}} \right) + \left[ 1 - 0.44 \left( 1 - \frac{S_{sb}}{S_{sb} + S_{tb}} \right) \right] \exp \left( -2.2 \frac{S_{sb} + S_{tb}}{S_m} \right)$ $S_{sb} = 0.00436 D_s L_{sb} (360 - \theta_{ds}), S_{tb} = \left\{ \pi/4 \left[ (D_t + L_{tb})^2 \right] \right\} N_t (1 - F_w)$ $S_m = L_{bc} \left[ L_{bb} + \left( (D_{ctl}/L_{tp,eff}) (L_{tp} - D_t) \right) \right], \theta_{ds} = 2 \cos^{-1} \left[ 1 - 2(B_c/100) \right]$
Tube bundle bypass CF ( $J_B$ )	Flows through bypass areas due to the gap between the shell wall and tube bundle	$J_B = \exp \left[ -C_{bh} F_{sbp} \left( 1 - \sqrt[3]{2r_{ss}} \right) \right]$ $F_{sbp} = \frac{S_b}{S_m}, S_b = L_{bc} \left[ (D_s - D_{out}) + L_{pl} \right], r_{ss} = N_{ss} / \left( (D_s/L_{pp})(1 - 2(B_c/100)) \right)$
Unequal baffle spacing CF ( $J_S$ )	The difference in inlet and outlet baffle spacing compared to the central ones	$J_S = \frac{(N_b - 1) + (L_{bi}/L_{bc})^{1-n} + (L_{bo}/L_{bc})^{1-n}}{(N_b - 1) + (L_{bi}/L_{bc}) + (L_{bo}/L_{bc})}$
Laminar flow CF ( $J_R$ )	The adverse temperature gradient formed in the boundary layer.	$J_R = (10/N_c)^{0.18} + ((20 - Re)/80) \left[ (10/N_c)^{0.18} - 1 \right]$ $N_c = (N_{icc} + N_{icw})(N_b + 1), N_{icw} = 0.8/L_{pp} \left[ D_s (B_c/100) - ((D_s - D_{ctl})/2) \right]$
Wall viscosity ( $J_\mu$ )	The variation in fluid properties between the bulk and the wall	$J_\mu = (\mu/\mu_{wall})^m \hat{U}_Y = \frac{dY}{dX} \hat{U}_X$

967

968 **Table A.3.**  
 969 Flow coefficients for flow stream analysis (Wills-Johnston) method [1].

Coefficient	Governing equation	Description
Combined flow coefficient ( $n_p$ , $n_a$ , $n_{cb}$ )	$n_p = 1 / (n_a^{-0.5} + n_s^{-0.5} + n_t^{-0.5})^2$ $n_a = n_w + n_{cb}, n_{cb} = 1 / (n_c^{-0.5} + n_b^{-0.5})^2$	The effect of different resistance coefficient over $\Delta P$ and h.
Shell-to-baffle leakage resistance coefficient ( $n_s$ )	$n_s = \frac{0.036(t_b / \delta_{sb}) + 2.3(t_b / \delta_{sb})^{-0.177}}{2\rho S_s^2}$ where $S_s = \pi (D_s - \delta_{sb})\delta_{sb}$	Shell-to-baffle flow resistance due to clearance between shell-to-baffle.
Tube-to-baffle clearance resistance coefficient ( $n_t$ )	$n_t = \frac{0.036(t_b / \delta_{tb}) + 2.3(t_b / \delta_{tb})^{-0.177}}{2\rho S_t^2}$ where $S_t = N_T \pi (D_s + \delta_{st})\delta_{st}$	Tube-to-baffle flow resistance due to clearance between tube-to-baffle.
Window flow resistance coefficient ( $n_w$ )	$n_w = \frac{1.9 \exp(0.6856 S_w / S_w)}{2\rho S_w^2}$	Due to mix the flow of cross and combine bypass flow.
Bypass flow resistance coefficient ( $n_b$ )	$n_b = \frac{a(D_s - 2L_c) / P_{TP} + N_{ss}}{2\rho S_b^2}$ where $S_b = (2\delta_{by} D_s + \delta_{pp})L_B$	The combined effect of the bundle and pass partition bypass streams.
Cross-flow resistance coefficient ( $n_c$ )	$n_c = \frac{N_c K_f}{2\rho S_m^2}$ $K_f = 0.272 + \frac{0.207 \times 10^3}{Re} + \frac{0.102 \times 10^3}{Re^2} - \frac{0.286 \times 10^3}{Re^3}$ for $3 < Re < 2 \times 10^3$ $K_f = 0.267 + \frac{0.249 \times 10^4}{Re} - \frac{0.927 \times 10^7}{Re^2} + \frac{0.10 \times 10^{11}}{Re^3}$ for $2 \times 10^3 < Re < 2 \times 10^6$	Obtained from the ideal bank correction factor and a function of cross-flow Reynold number. The parameter $K_f$ , for in-line square arrays.

970